REVIEW

Check for updates

Adsorptive and photocatalytic strategies for carmoisine removal: mechanisms, material innovations, and environmental implications

Muhammad Arif [ID] *

Carmoisine (CM) (also called azorubine or Acid Red 14) poses severe environmental and health risks due to its chemical stability, persistence in environment, and generation of toxic aromatic amines. Conventional treatment methods such as coagulation, oxidation, membrane filtration, and biological degradation are ineffective and can lead to secondary pollution and incomplete mineralization. Thus, adsorptive and photocatalytic processes have emerged as efficient and sustainable alternatives for CM removal. Adsorption enables rapid dye capture through surface interactions, while photocatalysis achieves complete degradation through light-induced reactive oxygen species. Their integration in adsorptive–photocatalytic composites enhances dye pre-concentration, promotes *in situ* degradation, and improves catalyst reusability. This review critically discusses the mechanisms, material types, and factors controlling these processes, with emphasis on the influence of surface chemistry, electronic properties, and operational conditions. It also addresses gaps in previous studies, including poor standardization, lack of real wastewater evaluation, and limited environmental assessment. The novelty of this work lies in its comprehensive analysis linking removal performance with mineralization efficiency, toxicity reduction, and scalability while proposing green synthesis and standardized evaluation approaches. Overall, this review provides a concise yet critical framework for advancing efficient, eco-friendly, and practical adsorptive–photocatalytic technologies for the removal of CM from contaminated water systems.

1 Introduction

Dyes are essential in modern industries such as textiles,[1] leather,[2] food,[3] cosmetics,[4] and plastics,[5] as well as in biomedical applications,[6] where they confer color, functionality and product identity. Among them, synthetic azo dyes such as carmoisine (azorubine or Acid Red 14) widely used as food[7] and textile[8] colorants are favored for their low cost, vivid color and facile application. However, the physicochemical stability that makes these molecules industrially useful (extended π-conjugation, sulfonate groups for water solubility and resistance to photodegradation) also renders them persistent in aqueous environments.[7,9,10] Therefore, effluent discharges from dyeing and related operations contribute colored plumes, which reduce light penetration in receiving waters, disturb photosynthetic ecosystems, and introduce complex organic molecules that resist conventional biological treatment. Thus, the ubiquity of dyes in commercial products generates concern. Dyes are functionally essential across sectors, yet their environmental release poses significant ecological and human-health risks.[11,12]

Carmoisine and related azo dyes exert toxicity through multiple pathways, including acute and chronic toxicity to aquatic organisms, formation of mutagenic and carcinogenic aromatic amines upon reductive cleavage, and endocrine-disrupting effects of certain degradation products.[13–15] In humans, exposure routes range from contaminated drinking water and food to occupational inhalation or dermal contact in dye-processing workers. Epidemiological and toxicological studies associate some azo dyes and their metabolites with genotoxicity, liver and kidney stress and other systemic effects.[16–18] In aquatic environments, dyes damage light-driven primary production, alter community structure, and bioaccumulate or transform into more toxic species under anaerobic conditions. These multi-faceted risks demand treatment technologies that do not simply hide color but actually eliminate toxicity and persistent organic load.

Traditional physicochemical and biological treatment methods, such as coagulation–flocculation,[19] chemical oxidation,[20] activated sludge,[21] filtration through membrane,[22] and adsorption on unmodified low-cost sorbents,[23] have been widely applied but have significant drawbacks. Coagulation and flocculation transfer pollutants into sludge, which requires further handling and is time-consuming. Chemical oxidants (chlorination and permanganate) can generate halogenated by-products, which are also toxic in nature. Membranes for

Department of Chemistry, School of Science, University of Management and Technology, Lahore 54770, Pakistan. E-mail: Muhammadarif2861@yahoo.com; Muhammadarif@umt.edu.pk

filtration can get clogged easily and produce concentrated waste that can cause environmental pollution. Simple biological treatments are often ineffective against highly recalcitrant, sulfonated azo compounds. The use of activated carbon is very effective; however, it is costly to regenerate and is not selective. These limitations underscore the need for advanced, selective, and sustainable routes that achieve not only color removal but also mineralization and low secondary pollution.

Adsorptive–photocatalytic processes have emerged as complementary advanced strategies that address many of the shortcomings of older methods. Adsorption (particularly on engineered carbonaceous,[24] polymeric[25] or hybrid[26] sorbents) shows rapid dye removal, operational simplicity, and applicability across a wide range of matrices and pH conditions. Modern adsorbents (functionalized carbons,[27] biochar,[28] MOF-derived carbons,[29] and tailored polymers[30]) exhibit increased selectivity and recyclability compared to raw activated carbon. Alternatively, photocatalysis enables the *in situ* generation of reactive oxygen species under light irradiation to oxidize or mineralize dye molecules, which introduce the possibility of complete detoxification without large chemical inputs.[31] When combined in adsorptive–photocatalytic composites, the two techniques work synergistically.[32] In this way, adsorption concentrates dyes at active sites, which improve the apparent reaction rates, while photocatalysis degrades the adsorbed molecules and regenerates the sorbent, minimizing secondary solid waste. Compared with older approaches, these modern methods promise higher removal efficiency, lower sludge generation, potential solar operation and modular reactor design suitable for remediation approaches.

The rapid increase in literature on adsorptive and photocatalytic removal of dyes shows the importance of this topic of research. Primarily, the previous review articles consist only of adsorptive or catalytic removal of dyes from water or use of specific materials to remove azo dyes, and these reports present general trends of dyes during their removal.[33–36] However, the removal of individual dyes through both adsorptive and photocatalytic processes varies due to differences in their interaction behaviors, molecular sizes, polarities, and structural properties. Also, there is a shortage of lifecycle and techno-economic perspectives, little scrutiny of regeneration energy and secondary waste management, and very limited synthesis of pilot-scale or real-waste evaluations. Few reviews integrate *operando* spectroscopic evidence or DFT-based insights linking material electronic structure to selective degradation pathways. These gaps hinder the translation of promising materials into safe and scalable technologies.

Therefore, there is a need for a review article that provides a critical and integrative appraisal going beyond performance lists such as systematically comparing adsorbents and photocatalysts based on metrics that are important for environmental safety (total organic carbon (TOC) removal, intermediate identification, and ecotoxicity), operational viability (regeneration energy, metal leaching, and recyclability), and scalability (solar-compatibility, reactor design implications, and cost drivers). This review provides mechanistic evidence (radical pathways and adsorption *vs.* surface reaction control) and assesses matrix effects (natural organic matter (NOM) and salts) with a focus on real wastewater conditions. Novel contributions include proposed standardized reporting guidelines for dye-remediation studies, a decision framework linking material properties to treatment train placement (pretreatment, main treatment, and polishing), and a techno-environmental outlook combining preliminary life-cycle considerations and suggestions for pilot demonstration protocols.

The adsorptive and photocatalytic removal of CM provides the most suitable path toward efficient, low-waste dye remediation, but progress requires a shift toward system-level thinking. These approaches provide rigorous evaluation of mineralization and toxicity, standardized experimental reporting, green material synthesis, and demonstration under realistic conditions. By addressing the methodological and translational deficiencies in prior reviews and providing a roadmap for integrated, lifecycle-aware research and scale-up, this review seeks to accelerate movement from laboratory innovation to robust, environmentally responsible deployment for dye-contaminated waters.

2 Synthesis, applications, and toxicity of carmoisine

Carmoisine (azorubine) is a synthetic azo dye widely used in various industries due to its intense red coloration, high water solubility, and cost-effectiveness. It is typically synthesized through an azo-coupling reaction between diazotized sulfanilic acid and 2-naphthol-3,6-disulfonic acid under controlled pH and temperature conditions, as shown in Fig. 1. This process involves diazotization of the aromatic amine using sodium nitrite in an acidic medium, followed by coupling with the activated aromatic compound to form the azo (–N=N–) linkage responsible for its characteristic color.[37] However, although this synthesis route is industrially efficient, it generates a large number of dye-laden effluents containing unreacted aromatic amines and sulfonated by-products, which contribute to significant environmental concerns.
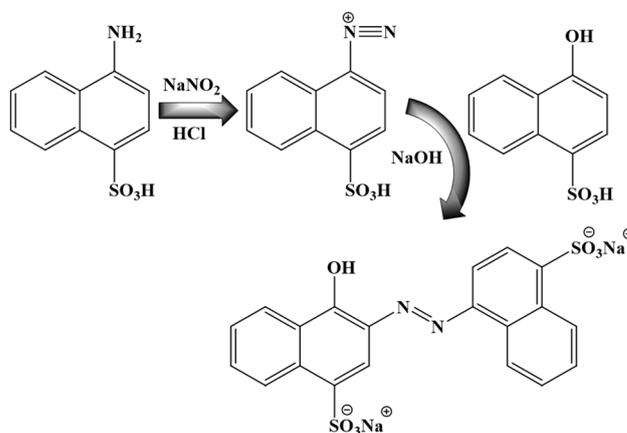

Fig. 1 Synthesis of carmoisine through diazotization method.

CM is extensively used as a colorant in beverages, candies, bakery products, textiles, leather, and personal care items.[38] However, its persistence, non-biodegradability, and strong affinity for organic matrices make it a potential pollutant in aquatic environments.[39,40] Toxicologically, CM and its degradation products (particularly aromatic amines) pose serious health risks such as allergic reactions, cytotoxicity, genotoxicity, mutagenicity, and carcinogenicity.[41,42] Several studies have demonstrated its potential to induce oxidative stress, DNA damage, and metabolic disturbances in aquatic organisms and human cell lines.[43,44] Its accumulation in water bodies interferes with light penetration, which disrupts photosynthetic processes and aquatic ecosystems, while its high stability under varying pH and temperature conditions complicates its natural degradation.[8,45]

Given these adverse effects, the removal of CM from water is of great environmental importance.[46] Conventional treatment methods are not effective due to their chemical stability and resistance to microbial attack. Therefore, advanced physicochemical and hybrid methods such as adsorption using biological and synthetic polymers, carbon derivatives, and their composites, photocatalysis employing metal oxides and metal sulfides, and advanced oxidation processes (AOPs), which involve hydroxyl radicals, have been widely explored. Among them, adsorptive–photocatalytic hybrid systems show better results, which enable both efficient dye capture and subsequent oxidative degradation into less toxic intermediates. Thus, the critical need for sustainable and efficient carmoisine removal technologies stems not only from its ecological persistence but also its potential to bioaccumulate and cause long-term health hazards, making it a key target in modern wastewater remediation research.

3 Mechanism of carmoisine removal

Different methods are used to remove CM from aqueous medium and each method has its own mechanism.

3.1 Adsorption removal

The adsorptive removal of CM is a complex physicochemical process involving multiple concurrent mechanisms that depend strongly on the surface chemistry and structure of the adsorbent, as well as on environmental parameters. CM molecules consist of extended conjugated π-electron systems, azo linkages (–N=N–), and sulfonate (–SO$_3^-$) groups, which render them both hydrophilic and negatively charged in aqueous media, as shown in Fig. 2(A–F). This structural duality allows diverse interaction modes with adsorbent surfaces. The
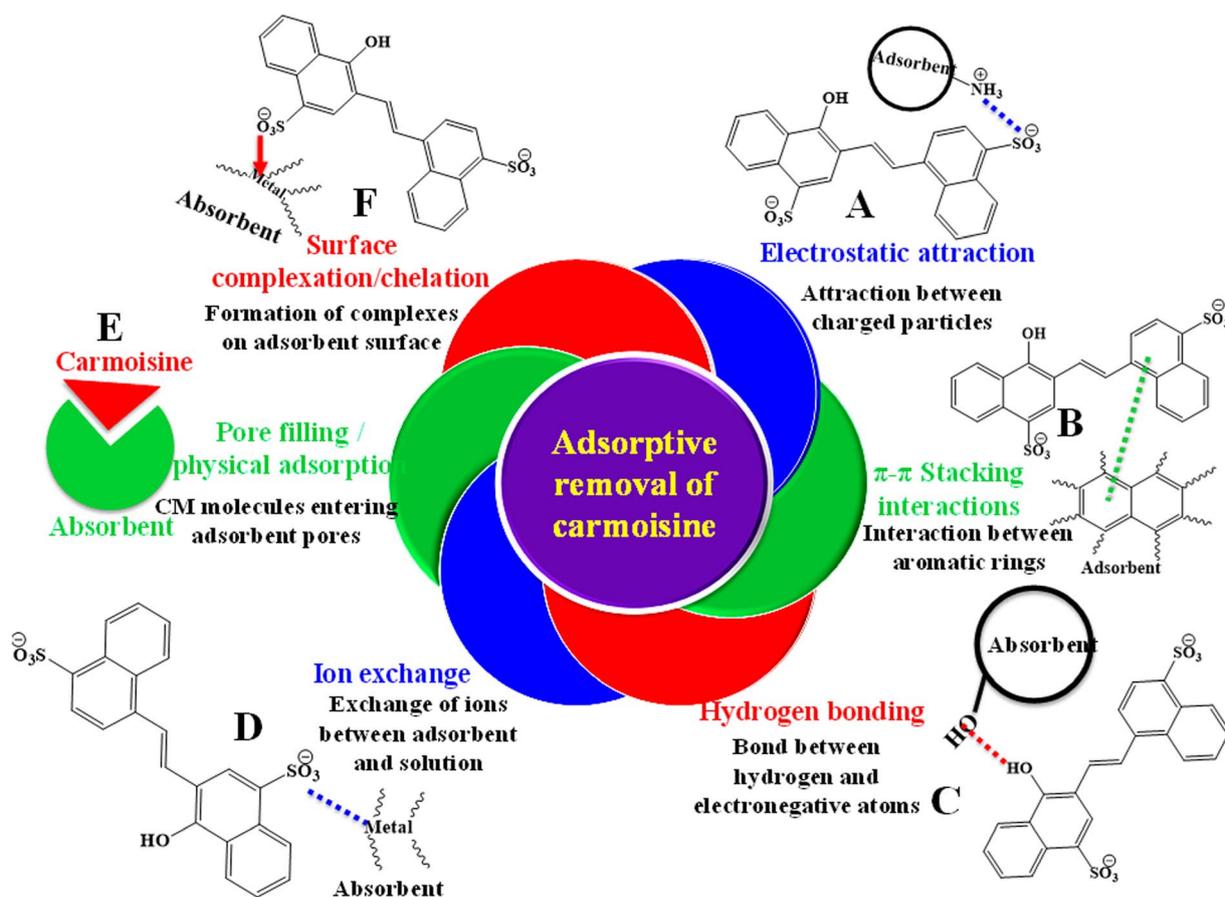

Fig. 2 Adsorption of carmoisine using an adsorbent through (A) electrostatic interaction, (B) $\pi-\pi$ stacking interaction, (C) hydrogen bonding, (D) ion exchange interaction, (E) pore filling/physical adsorption, and (F) surface complexation/chelation.

adsorption mechanism can broadly be classified into six overlapping types, as follows: (1) electrostatic attraction,[47] (2) π–π stacking,[48] (3) hydrogen bonding,[24] (4) ion exchange,[49] (5) pore filling/physical adsorption,[24] and (6) surface complexation/chelation.[30]

(1) Electrostatic interaction is one of the primary mechanisms when the adsorbent surface carries a positive charge (typically below its point of zero charge (pH_{pzc})), as shown in Fig. 2(A). Point of zero charge is the pH value of a medium at which the adsorbent surface possesses no net charge.[50–52] Alternatively, under conditions where the pH is above (pH > pH_{pzc}) or below (pH < pH_{pzc}), adsorbents have charges on their surface. At pH_{pzc} < pH of the medium, the functional groups of adsorbents are present in deprotonated form, which results in a negatively charged surface (such as $-COO^-$), together with neutral groups ($-NH_2$, $-OH$). Electrostatic repulsion occurs on the negatively charged adsorbent surface. At pH_{pzc} > pH of medium, the functional groups on the adsorbent surface are present in protonated forms such as $-NH_3^+$, $-OH_2^+$, or surface metal sites on oxides, which attract the negatively charged sulfonate groups of carmoisine through electrostatic interactions.[53] This mechanism dominates in biopolymers such as chitosan, amine-functionalized silicas, and cationic polymer composites.[54] Its efficiency is pH-sensitive; at high pH values, the adsorbent surface becomes deprotonated, leading to charge repulsion and decreased adsorption.

(2) π–π stacking and hydrophobic interactions occur between the aromatic π-electron system of carmoisine and the delocalized π-systems of graphitic adsorbents such as graphene oxide (GO), reduced graphene oxide (RGO), carbon nanotubes (CNTs), and biochar, as shown in Fig. 2(B). These interactions are non-electrostatic and remain effective across wide pH ranges, which make them valuable under conditions where electrostatic attraction weakens.[55] π–π stacking results in rapid adsorption kinetics and high dye affinity, but regeneration often requires solvent or oxidative treatment to disrupt the π–π associations.[56]

(3) Hydrogen bonding (Fig. 2(C)) plays a supportive but often decisive role, particularly in adsorbents with surface hydroxyl, amine, or carboxylic functionalities. The nitrogen atoms of azo linkages or oxygen atoms of sulfonate groups form hydrogen bonds with these surface groups, which lead to stable surface association. Although weaker than ionic bonding, the collective contribution of multiple hydrogen bonds enhances the adsorption strength and selectivity, especially in natural polymers and oxide-based materials.[25,57,58]

(4) Ion exchange is a mechanistically distinct pathway in which sulfonate groups displace anions (e.g., Cl^-, OH^-, and SO_4^{2-}) previously associated with positively charged sites on materials such as modified clays, zeolites, and ion-exchange resins,[29,59] as shown in Fig. 2(D). This results in stoichiometric replacement and can be confirmed by shifts in ionic concentration in solutions. It is typically a slower, diffusion-limited process but leads to more permanent retention of the dye due to inner-sphere complex formation.

(5) Pore filling or physisorption refers to the physical entrapment of dye molecules inside the pores of high-surface-area materials such as activated carbons, mesoporous silica, or MOFs, as shown in Fig. 2(E). The adsorption rate depends on the compatibility between the dye molecular size and pore diameter.[60,61] Micropores (<2 nm) favor high surface coverage but can restrict diffusion, while mesopores (2–50 nm) allow faster mass transfer and higher equilibrium capacities.

(6) Surface complexation or chelation is characteristic of metal oxides and doped nanocomposites (e.g., Fe_2O_3, TiO_2, ZnO, and metal–organic frameworks), as shown in Fig. 2(F). The nitrogen and oxygen donor atoms of carmoisine coordinate with exposed metal cations and form inner-sphere complexes.[62,63] This chemisorption process is typically irreversible and often coupled with photocatalytic degradation under light exposure, which converts the adsorbed dye into smaller, less toxic intermediates.[59]

Physisorption components (van der Waals, pore-filling, and weak π–π) are generally fast, reversible and entropy-driven, while chemisorption components (coordination, strong hydrogen bonding, and ion exchange that produces inner-sphere complexes) are slower, more specific and often enthalpy driven. Importantly, experimental distinctions between these mechanisms require corroborative spectral and surface analyses (FTIR shifts, XPS binding-energy changes, zeta potential, and desorption/regeneration behaviour). The reliance solely on isotherm fits (Langmuir/Freundlich) or kinetic models (pseudo-first/second order) can be misleading because these models are empirical and do not uniquely identify underlying molecular interactions.[27,64–66]

Each mechanism exhibits distinct advantages and limitations. Activated carbons and graphitic materials show excellent performance due to their high surface areas and π–π affinity, which result in high adsorption capacities.[24] However, their drawbacks include regeneration energy costs and poor selectivity for carmoisine in mixed dye effluents. Chitosan-based adsorbents provide high selectivity through electrostatic and hydrogen bonding interactions and are biodegradable, though they suffer from swelling and reduced stability in acidic media.[67] Functionalized clays and zeolites are low-cost alternatives but limited by their low surface area and slow ion-exchange kinetics.[68] Metal–organic frameworks (MOFs) show tunable pore environments and coordination sites, face hydrolytic instability and synthesis complexity.[69] Biochars and hydrochars provide sustainable, low-cost platforms, though their performance depends critically on their activation and surface modification.[70]

The transition between adsorption mechanisms can be influenced by multiple physicochemical parameters. Solution pH governs the charge states of both dye and adsorbent.[68] At low pH, protonation enhances electrostatic attraction, while at high pH, deprotonation reduces it and emphasizes π–π or hydrophobic interactions. Ionic strength and the presence of competing ions can screen electrostatic forces, shifting the dominant mechanism from ionic to non-ionic (π–π, hydrogen bonding). Temperature affects the thermodynamic favorability of physisorption (generally exothermic) versus chemisorption (endothermic).[25] Higher temperatures can transform a primarily physical adsorption system into a chemisorptive one

due to enhanced molecular mobility and reaction kinetics. Surface functionalization such as grafting amine, quaternary ammonium, or carboxyl groups can selectively tune the adsorption pathway toward ionic or covalent binding.[27] Similarly, adsorbent morphology and porosity determine whether adsorption proceeds by surface attachment or pore filling. The initial concentration of dye also plays a key role. At low concentrations, monolayer chemisorption dominates, while at higher concentrations, multilayer physisorption becomes more significant.

The adsorption removal of CM represents a multifaceted interplay among surface chemistry, environmental parameters, and material design. A deep mechanistic understanding enables the rational selection or synthesis of adsorbents capable of switching between mechanisms depending on operational needs. Rapid, reversible uptake occurs through π–π or physical adsorption or strong, permanent immobilization through ion exchange or chelation process. The current research trend emphasizes hybrid adsorbents combining these mechanisms such as chitosan-graphene oxide, metal oxide-biochar, or MOF-polymer composites. These composites integrate high capacity, structural tunability, and recyclability. Such mechanism-guided designs are essential for the development of sustainable, high-efficiency technologies for the removal of CM and other recalcitrant azo dyes from aqueous environments.

The percentage removal of CM by physical adsorption depends on the empty space present in the adsorbent. Greater available empty space enables the removal of more CM from the medium compared to chemisorption. However, a disadvantage of physisorption is that CM easily detaches from the adsorbent during recycling. In contrast, the detachment of CM does not occur in chemisorption during recycling. Nevertheless, the active sites of the adsorbent are not available for reuse due to irreversibly attached adsorbates.

3.2 Photocatalytic degradation

The photocatalytic removal mechanism of CM involves a complex interplay between photophysical and photochemical processes, in which light energy activates a semiconductor catalyst to generate reactive species capable of mineralizing the dye into harmless end products such as CO_2, H_2O, and inorganic ions (SO_4^{2-} and NO_3^-). When a semiconductor photocatalyst (typically a metal oxide or metal sulfide or doped g-C_3N_4) is irradiated with light energy equal to or greater than its band gap, electrons (e^-) in the valence band (VB) are excited to the conduction band (CB), which leave behind positively charged holes (h^+) in the VB, as shown in Fig. 3. This photoinduced charge separation forms the basis of the photocatalytic mechanism. The photogenerated holes can oxidize surface-adsorbed water or hydroxide ions to yield highly reactive hydroxyl radicals ($^\bullet OH$), while the electrons reduce dissolved oxygen to superoxide radicals ($^\bullet O_2^-$). These reactive oxygen species (ROS) (along with h^+) attack the azo (–N=N–) and aromatic structures of CM and break them down into smaller, less toxic intermediates such as aromatic amines, phenolic derivatives, and finally CO_2 and H_2O through successive
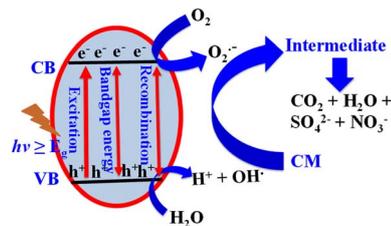

Fig. 3 Photocatalytic degradation mechanism of carmoisine by a semiconductor through the irradiation process.

oxidation reactions.[31,71,72] The overall efficiency depends on the balance among charge generation, separation, migration, and recombination.

The types of photocatalytic mechanisms can be broadly classified into (1) direct semiconductor photocatalysis, (2) photosensitized degradation, and (3) heterojunction or composite-based photocatalysis, each governed by different charge transfer dynamics.

3.2.1 Direct semiconductor photocatalysis. In direct semiconductor photocatalysis, the degradation of CM occurs through direct photoexcitation of a semiconductor material when irradiated with photons possessing energy equal to or greater than its band gap (E_g). Common photocatalysts (metal oxides, metal sulfide, and g-C_3N_4) undergo an intrinsic excitation process in which electrons (e^-) in the VB are promoted to the CB and leave behind positively charged holes (h^+) in the VB. The photogenerated electron–hole pairs migrate to the catalyst surface, where they participate in redox reactions with adsorbed species. The electrons in the CB reduce molecular oxygen (O_2) dissolved in water to generate $^\bullet O_2^-$, while the holes in the VB oxidize surface hydroxyl groups (–OH) or water molecules to produce $^\bullet OH$. These highly ROS initiate oxidative cleavage of the azo linkage (–N=N–) in CM, which leads to decolorization and further oxidation of the aromatic amines and sulfonated intermediates into CO_2, H_2O, NO_3^-, and SO_4^{2-}.[61,73]

The efficiency of direct photocatalysis depends on several key factors such as (i) light absorption ability (determined by the band gap and electronic structure of the semiconductor), (ii) charge separation and recombination rates, and (iii) surface adsorption capacity for CM molecules.[74,75] For example, TiO$_2$ (E_g = 3.2 eV)[76] and ZnO (E_g = 3.2 eV)[77] are highly efficient under UV light but exhibit a limited performance under visible light due to their wide band gaps. Furthermore, rapid electron–hole recombination in bulk materials drastically reduces the quantum efficiency. Thus, strategies such as metal or non-metal doping, coupling with narrow-bandgap semiconductors, and surface modification with carbonaceous materials have been employed to enhance their visible-light activity and prolong their charge carrier lifetime.
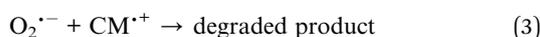
In direct photocatalysis, the degradation pathway is primarily governed by ROS-driven oxidation, which means that surface reactions rely on the continuous generation of $^\bullet OH$ and $^\bullet O_2^-$ radicals. However, excessive dye coverage or poor adsorption can hinder photon penetration and restrict access of CM molecules to the reactive sites, respectively, and hence reduce

the mineralization of CM. Thus, an optimal balance between adsorption affinity and photonic activation is crucial for achieving efficient degradation in direct photocatalytic systems.

3.2.2 Photosensitized degradation. In photosensitized photocatalytic degradation, the dye molecule itself acts as a photosensitizer under visible light. Because CM possesses an extended conjugated π-system with delocalized electrons, it absorbs visible light strongly (λ_{max} = 515–520 nm). This adsorption of visible light promotes an electron from its highest occupied molecular orbital (HOMO) to its lowest unoccupied molecular orbital (LUMO), which generates an excited singlet or triplet state (CM*), as shown in Fig. 4. This excited CM molecule can transfer the excited electron to the conduction band of the semiconductor, provided the LUMO of CM lies energetically above the CB of the photocatalyst. The transferred electron reacts with dissolved O_2 to form $^{\bullet}O_2^-$ radicals, while the oxidized dye cation radical (CM$^+$) undergoes self-oxidation, which decomposes into smaller fragments or reacts with other ROS such as $^{\bullet}OH$ to achieve further degradation.[39]

The photosensitization mechanism is represented in eqn (1)–(3).

$$CM* + semiconductor \rightarrow CM^{\bullet+} + e^-(CB) \tag{1}$$

$$e^-(CB) + O_2 \rightarrow O_2^{\bullet-} \tag{2}$$

$$O_2^{\bullet-} + CM^{\bullet+} \rightarrow degraded\ product \tag{3}$$

Unlike direct semiconductor excitation, the light absorption in photosensitized degradation arises from the dye, not the photocatalyst. Therefore, even wide-bandgap semiconductors (*e.g.*, TiO_2) can operate under visible light when CM acts as a sensitizer.[78] This mechanism is particularly relevant in real wastewater systems where colored dyes dominate visible-light absorption. However, the process is often self-limiting because once the sensitizing dye molecules are oxidized or desorbed, visible-light activity ceases. Moreover, degradation tends to produce partially oxidized intermediates unless accompanied by a secondary ROS-driven process.[79,80]

In practical terms, photosensitized degradation serves as an initiation mechanism that enhances electron injection and ROS generation under visible light, but it is rarely sufficient for complete mineralization on its own. To overcome this, composite systems combining photosensitization and direct photocatalysis have been developed. These systems enable CM

to act as a light harvester, while the semiconductor provides catalytic sites for radical formation and oxidation, resulting in higher overall efficiency.[80]

The direct photocatalytic mechanism is primarily semiconductor-driven, while the photosensitized mechanism is dye-driven. In direct photocatalysis, photons excite the semiconductor, while in photosensitization, photons excite the dye, which then injects electrons into the semiconductor. Direct photocatalysis generally ensures complete mineralization when sufficient light energy is available, while photosensitized systems offer visible-light activation but can result in partial degradation or surface fouling.[43,81]

The dominant mechanism can shift between these two pathways depending on several key parameters, as follows:

1. UV light promotes semiconductor excitation (direct mechanism), while visible light primarily excites the dye (photosensitization).

2. If the LUMO of the dye lies above the CB of the semiconductor, electron transfer occurs easily, which favors photosensitization, otherwise, direct photocatalysis dominates.

3. Strong dye adsorption enhances interfacial electron injection, which promotes photosensitization, while weak adsorption favors direct excitation.

4. High O_2 concentration supports the photosensitized pathway by accepting injected electrons to form $^{\bullet}O_2^-$ radicals.

5. The pH and surface charge also control these mechanisms. They affect the dye-surface affinity and thus determine which mechanism proceeds efficiently.

In real water treatment systems, both mechanisms coexist. CM first adsorbs onto the catalyst surface and can undergo photosensitized excitation under visible light, which initially generates radicals and partial degradation. Subsequently, direct photocatalytic oxidation driven by the semiconductor completes mineralization. Hence, efficient photocatalytic materials are engineered to integrate both pathways (combining strong light absorption, high surface area, and efficient charge separation) to achieve rapid, selective, and complete degradation of CM and other recalcitrant azo dyes.

3.2.3 Heterojunction or composite-based photocatalysis. The most advanced mechanism is heterojunction-based photocatalysis, which involves binary or ternary composites. Here, the interface between semiconductors with staggered or matched band structures facilitates efficient charge separation by forming type-I, type-II, Z-scheme, or S-scheme heterojunctions.

In advanced photocatalytic systems designed for efficient degradation of CM, the development of heterojunction photocatalysts has become a fundamental strategy to overcome the intrinsic limitations of single semiconductors, such as narrow light absorption range, rapid charge carrier recombination, and insufficient redox potential. By coupling two or more semiconductors with appropriately aligned energy band structures, electron–hole separation can be greatly enhanced, which boosts ROS generation and hence the overall degradation efficiency. Among these architectures, type-I, type-II, Z-scheme, and S-scheme heterojunctions represent the four most intensively studied and mechanistically distinct systems.
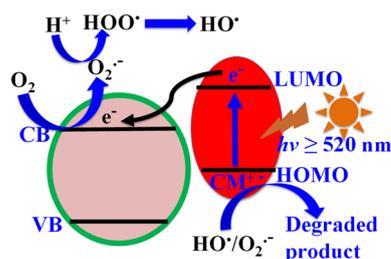

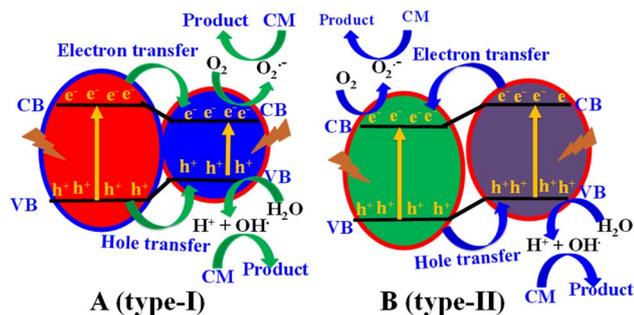Fig. 4 Direct photodegradation of carmoisine through irradiation.

Fig. 5 Photocatalytic degradation mechanism of carmoisine by two semiconductor composites through (A) type-I and (B) type-II.

Fig. 6 Mechanism for the photocatalytic degradation of carmoisine using (A) Z-scheme and (B) S-scheme semiconductor composites.

In type-I heterojunctions, two semiconductors are combined such that the CB of semiconductor A (red-colored material) lies at a higher energy (more negative potential) than that of semiconductor B (blue-colored material), and the VB of A (red color) is at a lower energy (high positive potential) than the VB of B (blue color), as shown in Fig. 5(A). When light excites both semiconductors, photoelectrons in the CB of A migrate to the lower CB of B, while photogenerated holes in the VB of A move to the higher VB of B. This spatial charge separation effectively reduces electron–hole recombination, which prolongs the carrier lifetime.

In type-II (staggered band) heterojunctions, two semiconductors are combined such that the CB of semiconductor A (purple colored material) lies at a higher energy (more negative potential) than that of semiconductor B (green colored material), and the VB of A is at a higher energy (less positive potential) than the VB of B, as shown in Fig. 5(B). When light excites both semiconductors, photoelectrons in the CB of A migrate to the lower CB of B, while photogenerated holes in the VB of B move to the higher VB of A. This spatial charge separation effectively reduces electron–hole recombination, which prolongs the carrier lifetime. For example, in a TiO_2–$CoFe_2O_4$ heterostructure, electrons transfer from $CoFe_2O_4$ (narrower bandgap) to TiO_2 (wider bandgap), while holes move in the opposite direction.[82]

However, despite its improved separation efficiency, the type-II mechanism suffers from reduced redox power because both transferred electrons and holes occupy energy levels of lower oxidative and reductive potential, respectively. As a result, the generation of highly oxidative ˙OH radicals or strongly reductive ˙O_2^- radicals can be suppressed. For CM degradation, this can lead to incomplete oxidation, which produces partially degraded intermediates rather than full mineralization. Therefore, while type-II systems favor charge separation, they compromise degradation completeness unless coupled with additional enhancements such as cocatalysts or conductive supports.[65]

Z-scheme heterojunctions were developed and named for their resemblance to the "Z" pattern of charge transfer first described in natural photosynthesis and used to preserve strong redox potential while preventing recombination.[83] In a Z-scheme system, two semiconductors with suitably aligned
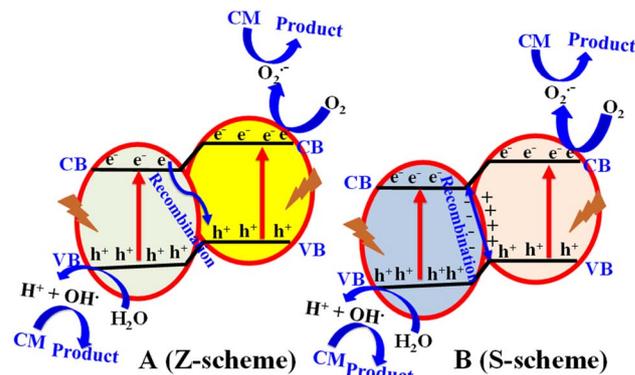
bands are connected through a solid-state conductor or by direct interface contact. Upon light irradiation, electrons in the CB of the less reductive semiconductor (B = light greyed material) recombine with holes in the VB of the less oxidative semiconductor (A = yellow colored material), as shown in Fig. 6(A). This selective recombination leaves behind electrons in the CB of A with strong reducing ability and holes in the VB of B with strong oxidizing power. Consequently, both charge carriers maintain their high redox potential, which enables the efficient formation of ˙O_2^- and ˙OH radicals simultaneously.

For instance, Nehru et al.[84] reported a g-C_3N_4–$NiCo_2S_4$ system that followed the Z-scheme mechanism for CM degradation. The electrons in the CB of TiO_2 recombine with holes from the VB of g-C_3N_4. The remaining electrons in the CB of g-C_3N_4 reduce O_2 to ˙O_2^-, while holes in the VB of $NiCo_2S_4$ oxidize H_2O or OH^- to ˙OH radicals. This dual radical generation leads to complete mineralization of CM into CO_2, SO_4^{2-}, and NO_3^-. Thus, the Z-scheme mechanism is superior to type-II in maintaining redox strength and suppressing photocorrosion. Nevertheless, its performance depends on the efficiency of the charge–transfer interface, where inefficient recombination at the junction can still lead to charge accumulation and slower kinetics.

The S-scheme heterojunction is a more recent conceptual model that refines the classical Z-scheme by integrating modern insights from band bending and internal electric field theory.[85] In the S-scheme, two semiconductors (typically an oxidation type (narrow bandgap) and a reduction type (wide bandgap)) are joined to form an internal electric field at their interface due to Fermi-level equilibration. Upon illumination, photogenerated electrons from the oxidation photocatalyst (with a low CB potential (light blue-colored material)) recombine with holes from the reduction photocatalyst (with a high VB potential (light orange-colored material)), similar to the Z-scheme, as shown in Fig. 6(B). However, recombination occurs naturally under the influence of the built-in electrostatic potential (internal electric field), without requiring an external mediator. The remaining electrons and holes are spatially separated on opposite sides of the junction, which maintain high reduction and oxidation potentials.

Unlike Z-schemes, which require conductive bridges, S-schemes achieve self-driven charge migration, making them more stable and structurally simpler. For CM degradation, S-scheme photocatalysts have shown superior visible-light activity owing to their effective charge separation, sustained redox power, and wide spectral absorption. The internal electric field ensures the directional migration of charge carriers, which results in a higher rate of ROS generation and more complete dye mineralization.

When comparing these systems, type-II heterojunctions excel in charge separation but sacrifice redox potential. Z-scheme systems retain strong oxidative and reductive abilities but require efficient recombination interfaces, while S-scheme heterojunctions combine both advantages (strong redox activity and robust charge separation) through intrinsic band bending. For CM removal, type-II structures can achieve moderate decolorization but often leave aromatic intermediates, whereas Z- and S-scheme systems typically yield near-complete mineralization with superior photostability.

The dominant photocatalytic mechanism can shift depending on the material parameters and operating conditions. Band alignment, work function differences, and Fermi-level positions dictate whether each composite exhibits type-II or S-scheme behavior. Interface quality (governed by synthesis route) also affects the charge transfer pathways. pH and ionic strength alter surface potentials and carrier migration by modifying band bending, while light wavelength influences which semiconductor is excited preferentially. Additionally, defect density, oxygen vacancies, and dopants can create intermediate energy levels that convert a conventional type-II interface into S-scheme-like behavior under certain illumination conditions.

The type-II, Z-scheme, and S-scheme heterojunction architectures represent the evolutionary stages of photocatalyst design aimed at optimizing the charge carrier dynamics. For CM and similar azo dye degradation, the S-scheme configuration currently offers the most promising balance of visible-light responsiveness, redox potential retention, and structural simplicity. Future advancements are expected to focus on precise interface engineering, defect modulation, and synergistic adsorption–photocatalysis coupling which enable the next generation of hybrid photocatalysts capable of complete dye mineralization under solar irradiation.

Upon visible light excitation, plasmonic nanoparticles (e.g., Ag or Au) produce high-energy ("hot") electrons through non-radiative localized surface plasmon resonance (LSPR) decay. These electrons can overcome the barrier at the metal-semiconductor interface and inject into the CB of a neighboring semiconductor, as shown in Fig. 7. The transferred electrons subsequently reduce O_2 to generate $\cdot O_2^-$, which attack the azo linkage (–N=N–) and aromatic rings of CM. Simultaneously, the residual hot holes remaining in the metal nanoparticle or trapped in the semiconductor valence band can oxidize surface hydroxyls or water molecules to yield $\cdot OH$ radicals, which lead to progressive oxidation and mineralization. This synergistic process enables plasmonic materials to extend the photocatalytic activity of wide-bandgap semiconductors into the visible region, substantially improving the degradation rate
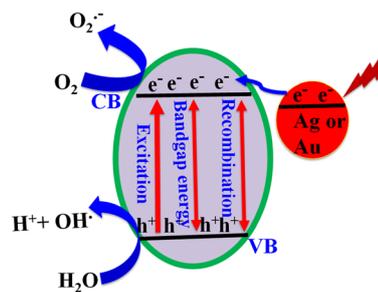

Fig. 7 Photocatalytic degradation mechanism of carmoisine by Ag- or Au-doped semiconductor.

under solar illumination. Similar results have been reported by Shams et al.[86] They applied Ag-doped g-C_3N_4 for the photocatalytic degradation of CM. They reported that the Ag-doped g-C_3N_4 showed high catalytic degradation (90%) compared to pure g-C_3N_4 under similar conditions owing to LSPR.

LSPR also induces a strong local electromagnetic field near the metal nanoparticle surface, which amplifies the effective photon flux around adjacent semiconductor sites. This intensified field promotes the excitation of more electron–hole pairs within the semiconductor and accelerates interfacial charge transfer. For CM, this localized field enhancement increases the generation of reactive oxygen species and enhances the degradation efficiency, particularly under low-intensity visible light.

In the plasmon-induced resonance energy transfer non-radiative energy transfer process, the energy of excited plasmons is resonantly transferred to the semiconductor without direct electron injection. When the LSPR energy matches the bandgap of the semiconductor, the oscillating plasmonic field excites electrons directly from the semiconductor VB to the CB. This mechanism is particularly dominant in core–shell nanostructures, where intimate contact and energy resonance facilitate continuous electron–hole generation, which sustains CM degradation even under weak visible illumination.

Direct TiO_2 and ZnO systems show robust oxidation power but are UV dependent and suffer rapid charge-carrier recombination which limit their quantum efficiency. Doped systems (non-metal[87] or metal-doped[73,88] semiconductor) enhance
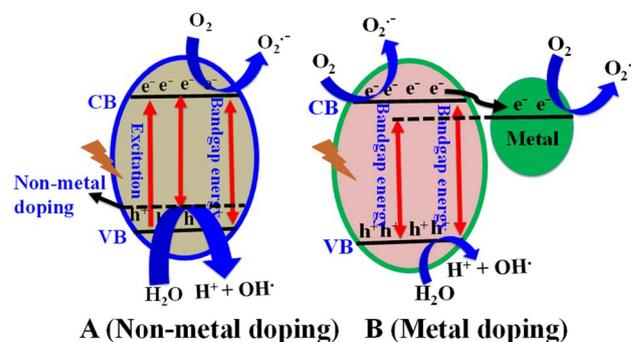

Fig. 8 Photocatalytic degradation mechanism of carmoisine by (A) non-metal-doped semiconductor and (B) metal-doped semiconductor.

visible-light activity by introducing intermediate energy levels, as shown in Fig. 8(A and B), respectively. In these doped systems, dopant stability and leaching can be issues. Heterojunction systems and doped semiconductors show the best photocatalytic performance by maintaining a strong redox potential and effective charge separation, yielding faster mineralization and lower intermediate toxicity.[89] Carbonaceous materials such as graphene, RGO, and carbon quantum dots incorporated into these systems serve as electron mediators, which reduce recombination and enhance dye adsorption through π–π interactions and hence accelerate the degradation kinetics. However, the complex synthesis and stability of composites in real wastewater matrices remain challenges.

The photocatalytic degradation of CM using carbonaceous material-semiconductor composites has emerged as a highly efficient and sustainable approach for the mineralization of this persistent azo dye. They show synergistic interactions between the conductive carbon matrix and the semiconductor component. Carbonaceous materials provide large surface areas, abundant π-electron sites, and high adsorption capacity, which enhance the pre-concentration of CM molecules near the photocatalyst surface and facilitate rapid electron transfer during photoreaction. When coupled with semiconductors, these composites form heterojunctions that suppress electron–hole recombination and extend visible-light absorption through π–π conjugation and interfacial charge transfer. The carbonaceous framework acts as an electron mediator, which accepts photogenerated electrons from the conduction band of semiconductors and transfers them to dissolved oxygen or dye molecules, as reported by Sunil and Mandal.[72] They generate ROS which are responsible for the oxidative cleavage of azo bonds (–N=N–) in CM. The degradation process involves stepwise breakdown of the aromatic rings and sulfonated intermediates, which eventually form CO_2, H_2O, and inorganic ions. Compared to pristine semiconductors, carbon-semiconductor hybrids exhibit improved photostability, reduced band-gap limitations, and higher quantum efficiency under solar or visible irradiation. These composites offer environmental advantages through reusability and minimized secondary pollution, yet challenges remain in maintaining interfacial stability and optimizing carbon-semiconductor coupling for scale-up applications.

Several factors influence and shift the dominant photocatalytic mechanism. Light wavelength and intensity determine whether bandgap excitation or photosensitization dominates. UV light favors direct photocatalysis, while visible light promotes sensitized or heterojunction-based processes. pH critically affects surface charge, dye ionization, and ROS generation.[90] At acidic pH, enhanced protonation of catalyst surfaces promotes electrostatic attraction and efficient oxidation, while under basic conditions, excessive hydroxide ions can scavenge holes and suppress activity. Dissolved oxygen concentration dictates electron scavenging efficiency, as O_2 serves as an electron acceptor forming $^{\bullet}O_2^-$ radicals.[20] Catalyst morphology and crystallinity modulate charge transport and surface reactivity. Adsorption–photocatalysis coupling is also crucial because strong dye adsorption ensures proximity to the

reactive sites, whereas weak adsorption limits electron transfer and slows degradation. Thus, surface functionalization or incorporation of adsorption-active supporters enhances the photocatalytic performance by pre-concentrating CM molecules near photogenerated ROS. The electron–hole recombination rate is another determinant because materials with intrinsic defects, surface oxygen vacancies, or heterojunction interfaces promote charge separation and shift the mechanism toward ROS-driven oxidation rather than direct hole oxidation.

The synergy between adsorption and photocatalysis governs real-world performance. In the initial stage, adsorption dominates, which enriches dye molecules on the catalyst surface. Subsequently, photoexcitation generates ROS that attack these adsorbed molecules. When adsorption is poor, the mechanism shifts toward bulk-phase degradation, which is diffusion-limited and less efficient. Conversely, excessive adsorption without adequate charge transfer can suppress photocatalysis owing to site blockage or light shielding. Therefore, optimal systems are engineered to maintain a balance between adsorption and photoactivity.

The photocatalytic degradation mechanism of CM is governed by the dynamic interaction among photogenerated charge carriers, reactive oxygen species, and dye molecules, modulated by catalyst composition, light energy, and environmental conditions. A critical understanding of these mechanistic transitions (among direct, sensitized, and heterojunction-mediated pathways) enables the realistic design of photocatalysts that exploit visible light, minimize recombination, and achieve complete mineralization. Future research emphasizes hybrid materials integrating broad-spectrum light absorption, high surface adsorption, and redox stability, which ensure the sustainable, efficient, and environmentally benign removal of CM and similar recalcitrant azo dyes from aquatic systems.

Table 1 provides a comparison among direct semiconductor photocatalysis, photosensitized degradation, and heterojunction/composite-based photocatalysis for dye removal from water.

3.3 Adsorptive–photocatalytic degradation

The adsorptive–photocatalytic degradation process is a synergistic water treatment mechanism in which physical concentration of pollutants and chemical oxidation occur in a coordinated manner within the same system. In the first stage, adsorption acts as a pre-concentration step. Pollutant molecules diffuse from the bulk solution to the surface of a porous photocatalyst or composite material and become attached through electrostatic attraction, hydrogen bonding, π–π stacking, or surface complexation. This step does not alter the molecular structure of the contaminant, as discussed in the adsorptive removal process, rather it increases the local pollutant concentration at the solid–liquid interface. By reducing the mass transfer resistance and positioning the molecules directly at the reactive surface, adsorption significantly enhances the efficiency of subsequent photocatalytic reactions. This adsorptive–photocatalytic degradation behavior

Table 1 Comparison of direct semiconductor photocatalysis, photosensitized degradation, and heterojunction/composite-based photocatalysis for dye removal

Factors	Photosensitized degradation	Direct semiconductor photocatalysis	Heterojunction/composite-based photocatalysis
Basic mechanism	CM absorbs visible light and becomes photo-excited, excited dye injects electrons into semiconductor conduction band	Semiconductor absorbs photons ($h\nu \geq$ band gap), generating electron–hole (e^-/h^+) pairs that form ROS	Two or more semiconductors (or semiconductor-carbon systems) form an interface that enhances charge separation and ROS generation
Light utilization	Utilizes visible light for CM excitation	Often limited to UV region (e.g., TiO_2 and ZnO)	Can extend to visible/solar spectrum through band alignment or plasmonic/carbon coupling
Charge separation efficiency	Dependent on CM stability and electron injection and can compete with recombination	Moderate, rapid e^-/h^+ recombination is common	Enhanced charge separation due to band alignment (type-II, Z-scheme, and S-scheme)
Role of dye	Acts both as pollutant and photosensitizer	Targets pollutant only	Only pollutant, catalyst system engineered for optimal activity
Advantages	Effective under visible light, low band-gap requirement	Simple system, well-understood mechanism, stable materials	Improved quantum efficiency, broader light absorption, reduced recombination, higher degradation rates
Disadvantages	Risk of incomplete mineralization, dye photobleaching rather than full degradation, instability of sensitizer	Limited visible-light response, recombination losses, lower solar efficiency	More complex synthesis, possible interfacial instability, higher preparation cost
Mineralization efficiency	Often partial degradation, intermediates may persist	Moderate, depends on ROS generation efficiency	Generally higher mineralization owing to sustained ROS production
Scalability	Less predictable in real wastewater, depends on dye absorption properties	Technically scalable but energy-intensive if UV required	Promising for solar-driven systems but requires durability validation

of polymer-semiconductors has been reported in one of my review articles.[91]

The photocatalyst generates electron–hole (e^-/h^+) pairs on light irradiation with energy equal to or greater than the band gap of the semiconductor component. The photogenerated holes (h^+) can directly oxidize adsorbed pollutants or react with surface-bound water/hydroxide ions to form hydroxyl radicals ($^\bullet$OH), while the photogenerated electrons (e^-) reduce dissolved oxygen to produce superoxide radicals ($^\bullet O_2^-$), as discussed in photocatalytic degradation section. These ROS are highly oxidative and attack the adsorbed pollutant molecules and break chemical bonds such as azo (–N═N–), aromatic rings, or other chromophoric structures. Through successive oxidation steps, complex organic molecules are converted into smaller intermediates and completely mineralized into CO_2, H_2O, and inorganic ions.[61]

The adsorptive–photocatalytic system provides several advantages over individual processes. Adsorption improves the reaction kinetics by increasing the available surface area and minimizing diffusion limitations. In turn, photocatalysis prevents saturation of the adsorbent by degrading the captured pollutants and hence regenerating the active sites *in situ* and extending the material lifespan. Moreover, the close proximity between adsorbed molecules and reactive oxygen species enhances the degradation efficiency and reduces the accumulation of toxic intermediates. Thus, the adsorptive–photocatalytic process is not merely an additive effect but a cooperative mechanism where physical enrichment and chemical transformation operate simultaneously to achieve

a higher removal efficiency, better mineralization, and improved sustainability. Few polymer-semiconductor composites have been reported for the photocatalytic degradation of CM, and further research is expected in the near future.

To clearly differentiate between the adsorptive removal, photocatalytic degradation, and adsorptive–photocatalytic degradation of CM, it is essential to distinguish them based on their mechanism, driving force, and final outcome, which are discussed in each section. Table 2 presents a comparison to differentiate the processes used for the removal of CM with different materials.

3.4 Biological degradation mechanism

The mechanism for the biological degradation of CM is a complex, redox-dependent process in which microbial and enzymatic pathways cooperate to convert this persistent compound into harmless end products. Mechanistically, degradation proceeds through two distinct but interdependent stages, as follows: (1) anaerobic azo bond reduction[92] and (2) aerobic oxidative mineralization. Each stage involves different microbial communities, enzyme systems, and environmental requirements, and their efficiency is profoundly influenced by pH, temperature, oxygen availability, and nutrient balance.

In the first stage (anaerobic), microorganisms such as *Pseudomonas aeruginosa* (*P.A.*), *Klebsiella pneumoniae* (*K.P.*), *Enterococcus faecalis* (*E.F.*), *Shewanella oneidensis* (*S.O.*), and *Clostridium* (*C*) species utilize CM as an electron acceptor during respiration in the absence of oxygen. The degradation

Table 2 Comparison among adsorptive removal, photocatalytic degradation, and adsorptive–photocatalytic degradation of CM

Parameter	Adsorption	Photocatalytic degradation	Adsorptive–photocatalytic degradation
Fundamental principle	Surface-based accumulation of CM onto a solid material	Light-driven chemical oxidation/reduction of CM using a semiconductor catalyst	Sequential and synergistic process, where CM is first adsorbed and then photo-catalytically degraded
Structural change of CM	No chemical change, CM remains intact	Molecular structure of CM is broken down into intermediates and potentially mineralized	Initially unchanged (adsorption), then chemically degraded under irradiation
Nature of process	Physical or chemical surface interaction (no bond cleavage of CM)	Photochemical reaction involving generation of reactive species	Integrated surface concentration followed by photochemical transformation
Reactive species involved	None (no radicals generated)	Hydroxyl radicals ($^{\bullet}$OH), superoxide radicals ($^{\bullet}O_2^{-}$), photogenerated holes (h^+)	Reactive oxygen species generated near adsorbed CM molecules, which enhance degradation efficiency
Driving force	Electrostatic attraction, hydrogen bonding, π–π interaction, van der Waals forces, or chemisorption	Photon absorption (energy $\geq$ band gap) producing electron–hole pairs	Both adsorption forces and photon-induced redox reactions
Outcome	CM transferred from water to solid phase	CM chemically transformed into smaller molecules or mineralized (CO_2, H_2O, and inorganic ions)	CM captured and subsequently destroyed which reduce risk of secondary pollution
Environmental impact	Risk of secondary waste if not regenerated properly	Potential for complete mineralization; energy-intensive if artificial light is used	Improved sustainability due to *in situ* regeneration and enhanced degradation efficiency
Limitation	Surface saturation and requires regeneration	Possible electron–hole recombination; energy requirement	Requires optimized material design to balance adsorption capacity and photocatalytic activity

initiates when azoreductase enzymes catalyze the reductive cleavage of the azo bond (–N=N–) using intracellular cofactors nicotinamide adenine dinucleotide (NADH) or nicotinamide adenine dinucleotide phosphate (NADPH) as electron donors. This reaction transfers electrons from the reduced coenzyme to the azo bond, which splits it into two amine-containing fragments.[93]

For CM, azo bond cleavage produces sulfanilic acid (*p*-aminobenzenesulfonic acid) and 1-amino-2-naphthol-6-sulfonic acid as the major intermediates, as shown in Fig. 9. These products are colorless but often toxic, mutagenic, and resistant to further reduction, which represents a key limitation of the anaerobic phase. The reaction proceeds efficiently under neutral to slightly alkaline pH and moderate temperatures (30–37 °C) after reduction and these conditions favor the stability and activity of azoreductase enzymes. However (in strictly anaerobic systems), these aromatic amines tend to accumulate, which causes secondary environmental toxicity.

In the second phase (aerobic), oxidative degradation and mineralization occur. Here, white-rot fungi (*e.g.*, *Phanerochaete chrysosporium* (*P.C.*), *Trametes versicolor* (*T.V.*), and *Pleurotus ostreatus* (*P.O.*)) and aerobic bacteria (*Comamonas*, *Acinetobacter*, and *Sphingomonas*) utilize extracellular oxidative enzymes such as *laccase*, *lignin peroxidase*, and *manganese peroxidase* to attack the aromatic amines generated from the first stage, as shown in Fig. 9. The enzymatic oxidation introduces hydroxyl groups into the aromatic rings, followed by ring-opening and decarboxylation reactions.

These oxidative enzymes are highly non-specific, which enable them to degrade a broad spectrum of aromatic

pollutants such as dye intermediates. The ring-cleavage products (such as catechol, hydroquinone, and maleic acid) are further metabolized through the tricarboxylic acid (TCA) cycle
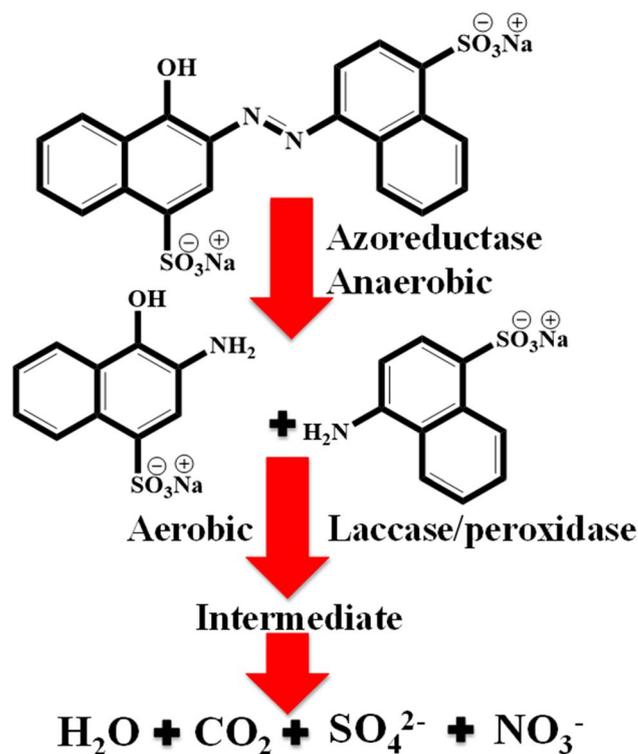

Fig. 9 Degradation mechanism of carmoisine by biological materials.

to achieve complete mineralization into CO_2, H_2O, NO_3^-, and SO_4^- ions. Thus, the overall degradation pathway of CM represents the synergistic coupling of anaerobic reduction and aerobic oxidation, where the first phase breaks the chromophore (responsible for color) and the second ensures detoxification and mineralization.[94]

From a critical mechanistic standpoint, this two-stage pathway is highly sensitive to environmental parameters. Dissolved oxygen (DO) and redox potential act as the primary regulators. At low DO, azoreductase activity is favored, whereas under aerobic conditions, peroxidase and laccase enzymes dominate. Hence, a shift from reductive to oxidative mechanisms occurs when oxygen or alternative electron acceptors (nitrate and sulfate) become available. The pH of the medium plays a dual role during these reactions. Under acidic conditions, it can protonate azo groups, which facilitates reduction, while neutral-to-slightly-alkaline environments favor microbial growth and enzyme stability.[95] Temperature affects the enzyme kinetics exponentially. However, high temperatures (>40 °C) denature key proteins, while low temperatures slow down metabolic activity. Nutrient availability (especially the presence of co-metabolites such as glucose, acetate, or yeast extract) influences the rate of electron transfer during the reductive phase. Low nutrient levels slow degradation, whereas excessive organics can suppress dye metabolism through substrate competition.

Environmental factors also dictate the pathway selectivity and toxicity outcome. In oxygen-limited sediments or anaerobic wastewater reactors, CM undergoes rapid decolorization, but the accumulation of aromatic amines increases the environmental risk owing to their carcinogenic and mutagenic potential. Conversely, aerobic systems prevent amine buildup but often fail to cleave the azo linkage completely, which facilitates partial degradation and color persistence. Therefore, sequential anaerobic–aerobic bioreactors are the most effective configuration, which ensure both chromophore breakdown and detoxification. Co-culture systems (combining bacteria and fungi) provide metabolic diversity, which enables simultaneous reduction and oxidation under microaerophilic conditions.

A comparative environmental assessment reveals that bacterial systems are kinetically efficient but environmentally incomplete unless coupled with oxidative treatment, while fungal systems are slower yet achieve higher detoxification. Algal systems integrate biosorption and biotransformation, but their efficiency is constrained by light availability and nutrient competition. Real wastewater conditions further modulate enzyme expression, biofilm formation, and microbial stability. For instance, metal cations can enhance laccase catalysis at trace levels but inhibit it at higher concentrations. Additionally, the presence of competing pollutants can divert metabolic energy and hence reduce the degradation efficiency.

The formation of aromatic amine intermediates during CM degradation was noted but requires deeper critical comparison with physicochemical treatment pathways. Under reductive or incomplete oxidative conditions, CM can generate sulfonated aromatic amines, which are more toxic, mutagenic, and persistent than the parent dye. These intermediates exhibit higher bioavailability and can resist further biodegradation due to stabilized aromatic structures. Therefore, processes that stop decolorization without full mineralization pose significant ecological risks. In contrast, advanced physicochemical oxidation methods (particularly well-optimized photocatalysis, photo-Fenton, ozonation, or sulfate-radical systems) aim to achieve complete mineralization through hydroxyl (˙OH) or sulfate ($SO_4^{\cdot-}$) radicals. These highly reactive species attack aromatic rings, which leads to ring opening, short-chain organic acids, and eventual conversion to CO_2, H_2O, NO_3^-, and SO_4^{2-}. However, the effectiveness of these systems depends strongly on the operational parameters and suboptimal radical generation can still result in partially oxidized aromatic fragments.

Physicochemical oxidation processes generally demonstrate superior mineralization capacity compared to purely reductive or adsorptive approaches, but they can incur higher energy or chemical inputs. Therefore, sustainable process design must balance complete degradation, intermediate toxicity suppression, and energy efficiency, which ensures that treatment does not substitute visible color removal for hidden toxic persistence.

3.5 Catalytic reduction/oxidation with metal nanoparticles

The catalytic reduction mechanism of CM by metal nanoparticles (MNPs) and their hybrids represents a highly efficient physicochemical approach in which the azo (–N═N–) linkage undergoes reductive cleavage through surface-mediated electron and proton transfer.[96] The process initiates when both the (reductant or oxidant) and CM molecules adsorb simultaneously on the catalyst surface. The metal surface acts as an electron relay, which transfer electrons from the reductant to the azo bond of the dye. The catalytic surface lowers the activation energy required for the reduction, which enables rapid cleavage of the azo linkage through successive hydrogenation steps that transform the azo (–N═N–) bond into hydrazo (–NH–NH–) intermediates, followed by scission into aromatic amines in the case of oxidation, as shown in Fig. 10. However, the azo group is converted into –N═NH and then N_2 and aromatic derivates in the oxidation process, as reported by Sohrabi *et al.*[97]
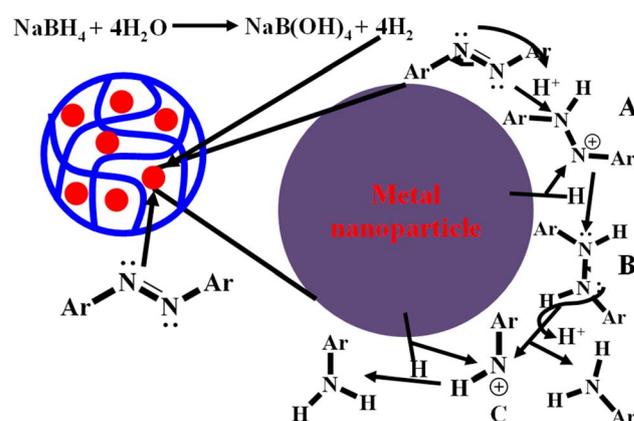

Fig. 10 Catalytic reduction mechanism of carmoisine by metal nanoparticles encapsulated by a support.

In this mechanism, adsorption is the key rate-determining step, and thus the physicochemical characteristics of the catalyst, including surface charge, crystallinity, facet exposure, and functionalization, strongly influence the catalytic activity. Smaller nanoparticles with high surface area-to-volume ratios exhibit enhanced catalytic activity due to their abundant active sites but suffer from aggregation and leaching, which can reduce their recyclability and increase environmental toxicity. Hybrid nanostructures such as metal-carbon composites overcome these challenges by offering synergistic effects. The support provides adsorption enrichment of dye molecules near the active sites, which enhances the charge transfer pathways and stabilizes metal nanoparticles against sintering or dissolution.[98] For instance, biochar and chitosan supports increase surface affinity through π–π interactions and electrostatic attraction, which facilitate dye proximity to the catalytic sites, while magnetic hybrids allow easy recovery from treated effluents, improving environmental safety and reusability.
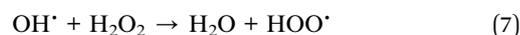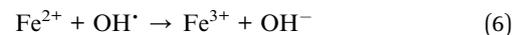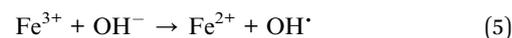
The reduction process achieves rapid decolorization, while it does not guarantee detoxification. The cleavage of the azo bond forms aromatic amines, which are more toxic, mutagenic, and carcinogenic than the parent dye. Hence, although catalytic reduction provides high kinetic efficiency and operational simplicity, it can produce environmentally persistent intermediates unless coupled with subsequent oxidative or biological mineralization stages. Comparatively, oxidative degradation or photocatalytic processes yield complete mineralization but often require external energy input and produce reactive oxygen species that can be scavenged by natural organics in wastewater. Conversely, MNP reduction is faster, less energy-intensive, and effective under mild conditions but must be integrated with advanced oxidation processes (AOPs) or bioremediation to achieve full detoxification.

From an environmental sustainability perspective, MNP-based reduction offers a high-efficiency treatment for industrial effluents but introduces new ecological risks. Leached metals can exert cytotoxic effects on aquatic microorganisms, disrupt the ecological balance, and persist in sediments. Noble-metal systems exhibit better chemical stability and recyclability but are economically and resource-wise unsustainable for large-scale use. Transition-metal and biopolymer-supported hybrids provide a greener alternative but often show slower kinetics and reduced durability under real wastewater conditions. Thus, to balance performance and sustainability, hybrid systems are increasingly engineered with magnetically recoverable cores, biogenic stabilizers, and recyclable supports, which minimize secondary contamination and maximize reuse.
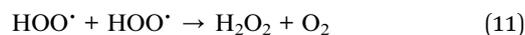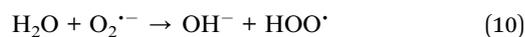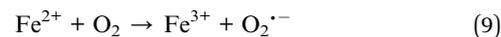
The catalytic reduction of CM by MNPs and their hybrids is a kinetically superior but environmentally incomplete pathway. They are excellent for rapid color removal but inadequate for full detoxification unless they are integrated into hybrid treatment systems. While environmental impacts can be mitigated through immobilization, recycling, and post-treatment, the inherent trade-off among speed, selectivity, and sustainability necessitates a holistic design approach that couples catalytic reduction with oxidation or biodegradation for the complete removal of CM from contaminated waters.

The oxidative degradation mechanism offers a more sustainable route as it leads to mineralization rather than partial reduction. In this pathway, transition metal nanoparticles or oxide hybrids activate oxidants such as H_2O_2 or O_2, which generate highly reactive radicals. In Fenton or Fenton-like reactions, Fe^{3+}/Fe^{2+} ions catalytically decompose hydrogen peroxide to produce hydroxyl radicals ($^{\bullet}OH$), as given by eqn (4)–(11).[99]

For the H_2O_2 oxidation reaction:

$$Fe^{2+} + H_2O_2 \rightarrow Fe^{3+} + OH^{\bullet} + OH^{-} \tag{4}$$

$$Fe^{3+} + OH^{-} \rightarrow Fe^{2+} + OH^{\bullet} \tag{5}$$

$$Fe^{2+} + OH^{\bullet} \rightarrow Fe^{3+} + OH^{-} \tag{6}$$

$$OH^{\bullet} + H_2O_2 \rightarrow H_2O + HOO^{\bullet} \tag{7}$$

$$HOO^{\bullet} + HOO^{\bullet} \rightarrow H_2O_2 + O_2 \tag{8}$$

For the oxygen oxidation reaction:

$$Fe^{2+} + O_2 \rightarrow Fe^{3+} + O_2^{\bullet -} \tag{9}$$

$$H_2O + O_2^{\bullet -} \rightarrow OH^{-} + HOO^{\bullet} \tag{10}$$

$$HOO^{\bullet} + HOO^{\bullet} \rightarrow H_2O_2 + O_2 \tag{11}$$

According to these equations, hydrogen peroxide reacts with ferrous ions to form ferric ions, hydroxide, and hydroxyl radicals, as shown in eqn (4). Hydroxide can further react with ferric ions to form ferrous ions and hydroxyl radicals, as provided in eqn (5). Fe^{2+} can donate an electron to the hydroxyl radical to form hydroxide and ferric ions. Hydroxyl radicals can also react with peroxide to form water and peroxide radicals, as in eqn (7). The peroxide radicals react with each other to form hydrogen peroxide and oxygen molecules.[100] In the case of oxidation with oxygen, ferrous ions donate electrons to oxygen molecules to form oxyradical anions and ferric ions, as provided in eqn (9). $^{\bullet}O_2^{-}$ reacts with water to produce peroxyl radicals and hydroxide and then the peroxyl radicals react with other peroxyl radical molecules to form hydrogen peroxide and oxygen molecules, as in eqn (10) and (11), respectively.

These radicals attack the azo bond and aromatic rings of CM, leading to ring opening, desulfonation, and stepwise oxidation into smaller carboxylic acids, which eventually mineralize to CO_2, H_2O, and inorganic ions. Hybrid nanostructures exhibit redox activity, adsorption capacity, and light response, which significantly enhance the degradation efficiency.[29] The surface interaction between the metal and semiconductor components allows electron–hole pair separation, suppresses recombination, and prolongs the charge lifetime, which are key factors in maintaining strong oxidative power.

In plasmonic or photocatalytic degradation systems, noble metal nanoparticles (Ag, Au) exhibit localized surface plasmon resonance (LSPR) when irradiated with light. The oscillation of conduction electrons generates "hot electrons" that can either transfer directly to the conduction band of a semiconductor or

interact with dissolved oxygen/water to produce ROS ($^{\cdot}O_2^{-}$ and $^{\cdot}OH$). The generated ROS initiate oxidative cleavage of the azo and aromatic structures of CM. Thus, plasmonic hybrids achieve dual-mode degradation of light-induced oxidative degradation and surface-mediated reduction.

4 Adsorptive and photocatalytic systems used for removal of carmoisine

Various adsorbent, catalytic, and photocatalytic materials have been reported for CM removal from aqueous solutions. These systems can be broadly categorized into inorganic (carbonaceous derivatives, porous silica, metal–organic frameworks, layer double hydroxides, and zeolites), organic and biopolymers. Their performance varies widely depending on their surface chemistry, porosity, and functionalization.

4.1 Inorganic adsorbent materials

Various types of inorganic materials have been used for the adsorptive removal of carmoisine, as shown in Fig. 11(A–I).

4.1.1 Carbonaceous materials. The adsorptive removal of CM using carbon-based materials is an essential strategy in wastewater purification due to its high efficiency, tunable surface properties, and environmental adaptability.[101] The mechanism primarily depends on the surface–solute interactions that occur between the aromatic azo dye and the physicochemical features of the carbon adsorbent. CM contains extended π-conjugated aromatic rings and sulfonate groups ($-SO_3^{-}$) that enable multiple adsorption pathways such as π–π stacking, electrostatic attraction, hydrogen bonding, and pore filling. The carbon framework (rich in delocalized π-electrons) interacts strongly with the aromatic π-system of the dye, which facilitates π–π electron donor–acceptor interactions, especially in graphene (Fig. 11(A)), graphene oxide (GO) (Fig. 11(B)), reduced graphene oxide (RGO) (Fig. 11(C)), and carbon nanotubes (CNTs) (Fig. 11(D)). Additionally, the functional oxygenated groups ($-COOH$, $-OH$, and $-C{=}O$) present on activated carbon, biochar, or oxidized graphene surfaces participate in hydrogen bonding and electrostatic attraction when the surface is positively charged under acidic conditions.

The adsorption efficiency is significantly influenced by surface area, pore volume, and surface functionality. Activated carbon (AC) (Fig. 11(E)) (with its extensive microporous–mesoporous network) exhibits high uptake capacities for CM through multilayer adsorption. However, its production from nonrenewable sources and energy-intensive activation (steam or CO_2
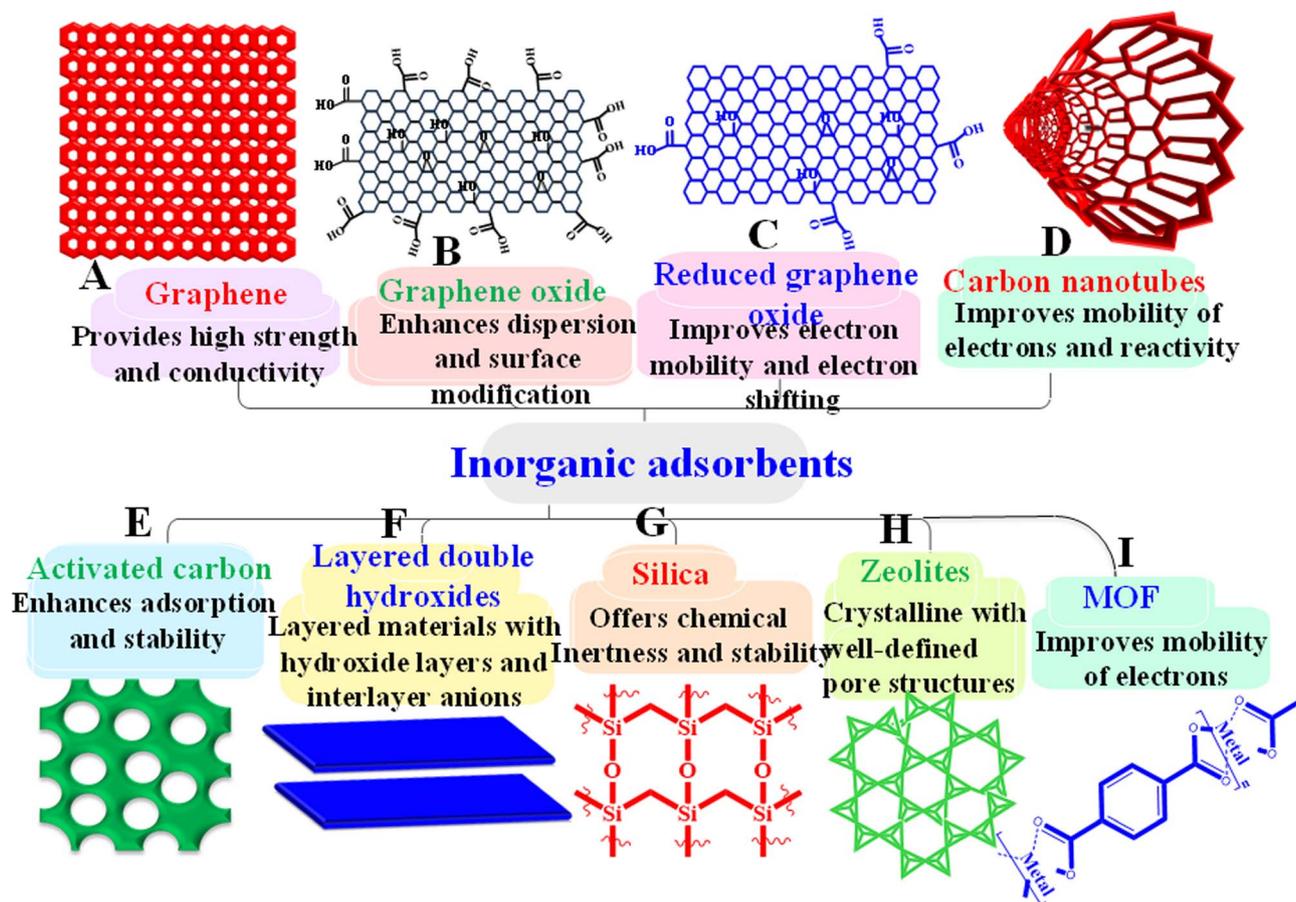

Fig. 11 Adsorptive removal of carmoisine by inorganic materials such as (A) graphene, (B) graphene oxide, (C) reduced graphene oxide, (D) carbon nanotubes, (E) activated carbon, (F) layered double hydroxides, (G) porous silica, (H) zeolites, and (I) metal–organic frameworks.

activation above 800 °C) raises environmental issues.[102] Biochar (BC) and hydrochar (HC) (derived from agricultural or algal biomass through pyrolysis or hydrothermal carbonization) represent green alternatives with good adsorption capacity (but less than AC) and the lowest carbon content.[103] Their surface contains diverse oxygen-containing groups that facilitate chemical adsorption and cation bridging. However, their irregular porosity and low graphitization reduce the adsorption kinetics compared to AC or graphene-based adsorbents. Conversely, graphene oxide (GO) and reduced graphene oxide (RGO) combine a two-dimensional π-conjugated structure with abundant oxygen functionalities, which allow both π–π stacking and electrostatic interactions. RGO (being partially restored to an sp² network) shows superior π–π interactions and higher affinity for aromatic pollutants, while GO (containing high polar functional groups) shows better electrostatic interaction with the polar parts of pollutants. CNTs provide tubular nanospaces and hydrophobic graphitic walls ideal for van der Waals and π–π adsorption, though their dispersion and surface oxidation determine their real-world performance.[104] Hybrid composites integrate adsorption with magnetic recovery or photocatalytic regeneration, which mitigates adsorbent disposal issues.[105]

Adsorption proceeds through two main stages, as follows: (1) film diffusion or boundary-layer transfer of dye molecules to the adsorbent surface and (2) intraparticle diffusion into pores or binding onto surface sites. The kinetics often follow pseudo-second-order models, which indicate dominant chemisorption involving valence forces and sharing or exchange of electrons. The adsorption equilibrium is typically described by Langmuir or Freundlich isotherms depending on surface homogeneity.[106] Langmuir behavior (monolayer adsorption) is typical for activated carbon and graphene, while Freundlich behavior (heterogeneous, multilayer adsorption) is common in BC and HC.[107] The thermodynamic parameters ($\Delta G°$, $\Delta H°$, and $\Delta S°$) often reveal the process as spontaneous and endothermic, which suggests increased randomness at the solid–solution interface and enhanced adsorption at higher temperatures.

Although carbon-based adsorption rapidly removes color and organic load, it merely transfers the contaminant rather than degrading it, which poses potential secondary pollution risks if the spent adsorbent is not treated or regenerated. Regeneration through heating, solvent extraction, or oxidation (using ozone or H_2O_2) can lead to structural collapse, pore blockage, or loss of active sites, which result in a gradual decline of performance after multiple cycles. Furthermore, desorbed CM or by-products during regeneration can re-enter the environment if not properly controlled. Therefore, adsorption should be seen as an intermediate or complementary process, ideally integrated with photocatalytic or biological oxidation for complete mineralization.[108]

Environmental factors play a decisive role in adsorption behavior. pH is the most influential factor. Acidic conditions enhance the protonation of carbon surfaces, which favor attraction toward anionic dyes such as CM. Conversely, at higher pH, electrostatic repulsion dominates, which shifts the mechanism from electrostatic interaction toward π–π stacking. Ionic strength reduces the adsorption efficiency by compressing the electrical double layer and competing for adsorption sites, while temperature positively affects the adsorption kinetics by enhancing dye diffusion. Natural organic matter (NOM) and co-existing anions (Cl^-, SO_4^{2-}, and NO_3^-) in wastewater can either block the active sites or alter the hydrophilicity of the adsorbent surface. In real wastewater, multi-component competition reduces the adsorption efficiency compared to pure laboratory systems, which reveals the importance of surface modification and hybrid system design for practical implementation.

Activated carbon exhibits an excellent performance but has a high environmental cost owing to its energy-intensive production and limited regeneration life. BC and HC are low-cost, carbon-negative materials that sequester CO_2 and repurpose agricultural waste but exhibit lower adsorption capacities and slower kinetics. Graphene and CNTs achieve exceptional adsorption capacities and tunability but suffer from high synthesis cost, scalability issues, and potential ecotoxicity if nanoparticles leach into ecosystems.[109] Thus, while graphene-based adsorbents are superior in terms of efficiency, biochar and hydrochar excel in sustainability, which makes them preferable for large-scale applications.

The adsorption of CM onto carbon-based materials is a physicochemical process with high efficiency but limited permanence. Its strength lies in its versatility, tunability, and rapid color removal, while its weakness stems from pollutant transfer rather than degradation. Thus, to ensure both environmental safety and long-term efficiency, the next generation of carbon-based adsorbents should focus on biogenic synthesis, magnetic recoverability, and hybrid integration with catalytic or biological systems. These strategies can transform adsorption from a mere containment process into a regenerative, circular, and environmentally sound water purification pathway for the sustainable removal of CM and similar recalcitrant dyes.

4.1.2 Other inorganic adsorbent materials. The adsorptive removal of CM using advanced porous inorganic materials such as layered double hydroxides (LDHs) (Fig. 11(F)), porous silica (PS) (Fig. 11(G)), zeolites (ZL) (Fig. 11(H)), and metal–organic frameworks (MOFs) (Fig. 11(I)) has gained tremendous attention because these materials have high structural tunability, chemical stability, and surface functionality, which enable the selective capture of complex anionic pollutants such as CM. Each class exhibits distinct adsorption mechanisms arising from differences in their surface charge, porosity, chemical functionality, and framework flexibility, which critically influence their performance, regeneration potential, and environmental sustainability.

Layered double hydroxides (LDHs), often represented as $[M_{1-x}^{2+} M_x^{3+}(OH)_2]^{x+}(A^{n-})^{x/n} \cdot mH_2O$ (where M^{2+} and M^{3+} are divalent and trivalent metal cations, respectively, and A^{n-} is an interlayer anion), possess positively charged brucite-like layers and exchangeable interlayer anions. For anionic dyes such as CM (bearing $-SO_3^-$ groups), their removal occurs primarily through anion exchange, electrostatic attraction, and intercalation into interlayer galleries. LDHs show high affinity under neutral to basic pH, where their interlayer anions (e.g., CO_3^{2-} and NO_3^-) are readily replaced by dye anions, which leads to the formation of stable dye-layer composites.[110] Under acidic

conditions, LDHs undergo partial dissolution and release metal ions (Al^{3+}, Zn^{2+}, and Mg^{2+}), which not only decreases their adsorption capacity but can also cause secondary metal contamination. Despite this, calcined LDHs can exhibit a "memory effect," wherein upon hydration they reconstruct and re-adsorb anions, which enhances their recyclability. Therefore, LDHs show fast adsorption kinetics and high selectivity but face pH sensitivity and structural instability in real wastewater environments, particularly under acidic or high ionic strength conditions.

Porous silica materials such as mesoporous MCM-41, SBA-15, and functionalized silicas rely on pore-filling, hydrogen bonding, and surface complexation mechanisms. Their ordered mesoporous channels provide high surface areas and uniform pore geometries, which allow the efficient diffusion of dye molecules. Bare silica surfaces are covered with silanol (Si–OH) groups that can hydrogen bond with the sulfonate or azo groups of dyes, but because silica is slightly negatively charged at neutral pH, surface functionalization is required to improve its anionic dye adsorption. Amine-functionalized silicas ($-NH_2$ and $-NR_3^+$) can strongly interact with CM through electrostatic attraction and hydrogen bonding. These modifications significantly increase their adsorption capacity, as reported by Sadeghi et al.[111] They used an Fe_3O_4 and amino-functionalized silica composite for the adsorption of CM in different pH media. They reported that the adsorption capacity of the composite decreases continuously with increasing pH from 2 to 6 owing to the shifting of the protonated amino ($-NH_3^+$) form to deprotonated form ($-NH_2$), which results in a decrease in interactions between the composite and negatively charged CM. Furthermore, the chemical inertness of silica and its easy regeneration through solvent washing or low-temperature heating make it environmentally robust. However, its synthesis is energy-intensive, and the surfactant templating agents used in the preparation of mesoporous silica can be toxic, which require thorough removal to prevent environmental harm.

Zeolites (crystalline aluminosilicates with microporous structures and tunable Si/Al ratios) remove CM primarily through electrostatic attraction and ion exchange at the cationic framework sites (Na^+ and Ca^{2+}). Their negative framework charge attracts cationic species.[61] However, since CM is anionic, its adsorption by zeolites often depends on their surface modification or the introduction of cationic functional groups. The adsorption mechanism can also involve pore-filling and external surface adsorption when the molecular dimensions of the dye exceed their pore spaces. Natural zeolites have lower surface areas but are cost-effective and highly stable under harsh chemical environments, which make them excellent for industrial wastewater treatment. Synthetic zeolites with hierarchical porosity (micro-mesoporous hybrid structures) exhibit enhanced diffusion and adsorption capacity. However, molecular size exclusion remains a limitation. Large aromatic dyes cannot access microporous sites. Zeolites are chemically and thermally stable and can be regenerated by mild heating, which produces minimal secondary waste. Environmentally, they are some of the most benign and recyclable adsorbents, but their

performance can decline in multicomponent wastewater due to competition and pore blocking.

Metal–organic frameworks (MOFs) represent the most advanced class of adsorbents for CM removal owing to their extraordinary porosity, tunable chemistry, and functionalizable organic linkers. MOFs exhibit large specific surface areas and accessible coordination sites that enable multiple interactions such as π–π stacking between aromatic dye rings and MOF linkers, hydrogen bonding, and metal–ligand coordination between dye functional groups ($-SO_3^-$ and $-N{=}N-$) and unsaturated metal sites.[48] Functionalization with amine or hydroxyl groups enhances the affinity toward anionic dyes through electrostatic attraction. For example, amine-functionalized MOFs show strong dye adsorption via hydrogen bonding and electrostatic forces.[112] However, many MOFs suffer from hydrolytic instability in aqueous environments, which leads to their structural collapse and metal ion leaching. This raises environmental safety concerns. Moreover, large-scale MOF synthesis often involves toxic solvents and high energy inputs, which limit their sustainability. Thus, strategies such as post-synthetic modification, polymer encapsulation, and formation of MOF-carbon composites are increasingly applied to improve their stability, recovery, and reusability.[113]

From an environmental and performance perspective, a critical comparison reveals distinct trade-offs. LDHs are efficient and selective but environmentally sensitive (acid dissolution and metal leaching). Porous silicas are chemically stable but require costly functionalization and regeneration energy input. Zeolites are highly durable and reusable but limited by their small pores and low affinity for bulky anionic dyes without modification. MOFs exhibit excellent capacities and selectivity but have complex synthesis, stability issues, and potential metal toxicity. In real wastewater, environmental factors such as pH, ionic strength, temperature, and competing ions strongly affect all these systems. Acidic conditions reduce the stability of LDHs and MOFs, while high ionic strength suppresses electrostatic adsorption in zeolites and silica. Temperature typically enhances the adsorption kinetics but can promote desorption or framework distortion in MOFs.

All four materials exhibit strong potential for the adsorptive removal of CM, while their environmental performance and sustainability vary significantly. LDHs and zeolites are most suited for large-scale, low-cost applications due to their chemical simplicity and recyclability. Porous silicas provide tunable and clean adsorption but with moderate sustainability challenges, while MOFs offer unmatched tunability and capacity but raise concerns about hydrolytic stability, toxicity, and life-cycle impacts. The most effective and environmentally sound approach is hybrid integration to leverage high capacity with improved stability and low environmental risk. Therefore, a rational, lifecycle-conscious design that balances efficiency, stability, and environmental compatibility is critical for deploying these advanced adsorbents in sustainable CM removal from aqueous systems.
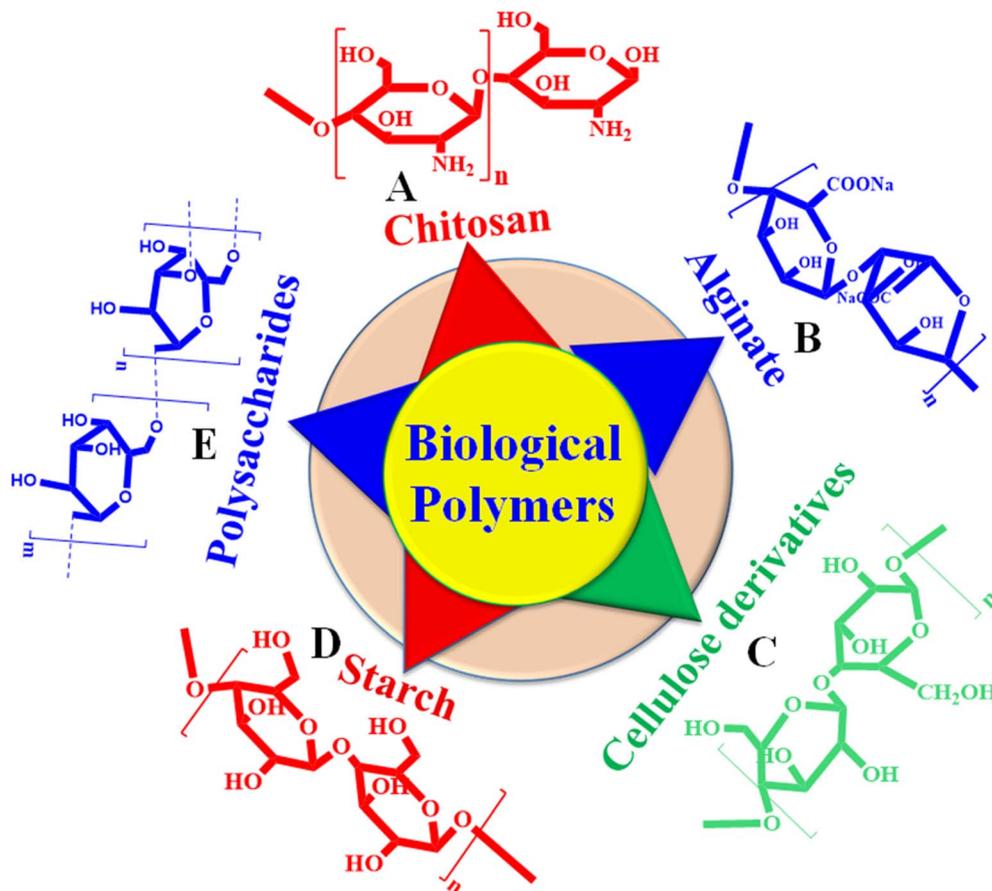
Fig. 12 Adsorptive removal of carmoisine by biological polymers such as (A) chitosan, (B) alginate, (C) cellulose derivatives, (D) starch, and (E) polysaccharides.

4.2 Biological polymers

The adsorptive removal of CM by biological polymer-based materials has emerged as a sustainable and environmentally friendly strategy owing to their natural abundance, non-toxicity, biodegradability, and capability to host diverse functional groups.[103] Polymers such as chitosan (CS) (Fig. 12(A)),[114] alginate (AN) (Fig. 12(B)),[115] cellulose derivatives (Fig. 12(C)),[116] starch (Fig. 12(D)),[117] and other polysaccharides (Fig. 12(E)) or protein-based matrices exhibit multifunctional adsorption mechanisms involving electrostatic attraction, hydrogen bonding, van der Waals interactions, and π–π stacking, which depend on their chemical composition and surface modification. Among them, chitosan (a deacetylated derivative of chitin) is the most widely studied biosorbent for anionic dyes such as CM because of its amino groups that become protonated ($-NH_3^+$) under acidic to neutral pH, resulting in strong electrostatic interaction with the sulfonate ($-SO_3^-$) groups of the dye. This interaction is complemented by hydrogen bonding between the hydroxyl groups (–OH) on chitosan and azo ($-N=N-$) or aromatic sites on the dye, which produces a multi-interaction network that enhances the binding stability.[118] However, pure chitosan has low mechanical strength, is soluble in acidic media, and exhibits limited surface area, which restricts its adsorption kinetics and reusability. Therefore, chemical crosslinking or composite formation with inorganic fillers is employed to improve its stability, surface area, and magnetically assisted recovery.

Alginate-based adsorbents (usually in the form of Ca-alginate beads or aerogels) operate primarily through ionic complexation and entrapment mechanisms. Their negatively charged carboxylate ($-COO^-$) groups can bind metal ions that act as bridges for dye molecules or be functionalized with cationic agents to attract anionic dyes such as CM.[115] However, native alginates tend to repel CM because of the electrostatic repulsion between their negatively charged groups. Thus, crosslinking and functionalization are essential to enhance their adsorption efficiency. Cellulose and its derivatives particularly carboxymethylcellulose, hydroxyethylcellulose, and aminated cellulose possess high hydrophilicity, chemical tunability, and large surface area.[119] Aminated cellulose interacts strongly with CM through electrostatic attraction and hydrogen bonding, while aromatic-functionalized cellulose adds π–π stacking interactions, which enhance its selectivity toward azo dyes.

Starch and cyclodextrin-based adsorbents exploit host–guest inclusion mechanisms, wherein the hydrophobic cavities of cyclodextrin molecules encapsulate aromatic dye molecules such as CM, driven by hydrophobic and van der Waals forces.[55,117] Meanwhile, protein- or peptide-based adsorbents

rely on amide and carboxyl groups for hydrogen bonding and electrostatic attraction. Although these materials show a lower dye capacity compared to chitosan-based systems, they provide biodegradability and natural abundance advantages. The adsorption performance among these materials is strongly governed by pH, ionic strength, and temperature. At lower pH values, protonation enhances the cationic site density in chitosan and aminated cellulose, thus improving CM uptake. Conversely, at higher pH, deprotonation reduces charge-based binding, which shifts the mechanism toward hydrogen bonding or π–π stacking. Elevated ionic strength causes charge screening, which reduces electrostatic interactions, while higher temperature often enhances dye diffusion and intra-particle penetration, increasing the equilibrium capacity but potentially weakening non-covalent interactions.

Chitosan-based adsorbents exhibit the highest adsorption capacities owing to their strong cationic sites and tunable hybridization potential.[114] Alginate[115] and cellulose derivatives show moderate capacities (less than chitosan-based adsorbents but higher than other bioadsorbents), which can be enhanced by grafting amine or aromatic groups. Starch and protein-based[120] materials generally exhibit lower capacities than alginate-based and chitosan-based adsorbents, but they offer low cost and biodegradability. When integrated into nano-composite systems, these biopolymers not only adsorb CM efficiently but can also act as support matrices for photo-catalytic or redox-active nanoparticles, resulting in adsorptive–photocatalytic dual functionality. This is a critical advantage for complete dye mineralization.

Biopolymer-based adsorbents have notable benefits compared to inorganic or synthetic polymeric systems. They are renewable, require low energy for their synthesis, and are biodegradable, which reduces their overall environmental impact. Furthermore, their degradation products are generally benign, which poses minimal ecotoxicity risks. However, their biodegradability can become a limitation when structural degradation occurs prematurely during their use, resulting in mechanical instability and potential desorption of the bound CM back into the environment. Furthermore, the disposal of dye-loaded biosorbents requires careful management. If incinerated or improperly composted, the adsorbed azo dyes can release toxic aromatic amines, thus negating their ecological benefits.

Chitosan-based systems show higher environmental stability and lower regeneration waste than alginate or cellulose systems, though they can still release amine-based residues in acidic environments. Alginate and cellulose are more environmentally benign but less efficient, which require modification steps that often involve chemical crosslinkers with moderate toxicity. Hybrid composites containing magnetic or metal oxide nano-particles can improve recyclability but introduce metal leaching risks, which raise ecological concerns if not properly encapsulated.

The adsorptive removal of CM by biological polymer-based materials represents an excellent balance between efficiency and environmental compatibility. Chitosan remains the benchmark due to its high cationic charge density and

modifiability, while cellulose and alginate offer greener, cost-effective alternatives. However, its practical deployment requires addressing stability-biodegradability trade-offs, regeneration efficiency, and secondary pollution control. Future research must focus on bio-derived crosslinking strategies, composite reinforcement with eco-safe nanoparticles, and closed-loop regeneration processes to achieve sustainable, high-performance adsorbents for real-world CM remediation.

4.3 Synthetic organic polymers

The adsorptive removal of CM using synthetic organic polymer-based materials represents a highly engineered approach that combines molecular design precision, surface functionalization, and structural tunability to achieve efficient, selective, and reusable dye removal. These materials (such as ion-exchange resins, quaternized or aminated hydrogels, conducting polymers (polyaniline, polypyrrole, and polythiophene), molecularly imprinted polymers (MIPs), hyper-crosslinked polymers (HCPs), covalent organic frameworks (COFs), and conjugated microporous polymers (CMPs)) show distinct adsorption mechanisms depending on their composition and architecture. Fundamentally, these polymers rely on electrostatic interactions, π–π stacking, hydrogen bonding, van der Waals forces, and pore-filling effects to capture CM, a complex anionic azo dye with sulfonate groups and aromatic rings that facilitate both ionic and π–π interactions.[121]

The most common mechanism is electrostatic ion exchange, in which positively charged sites (*e.g.*, quaternary ammonium, protonated amine, or imidazolium groups) on the polymer framework attract the negatively charged $-SO_3^-$ groups of CM. These materials (exemplified by anion-exchange resins and quaternized polymer hydrogels) display rapid uptake, high capacity, and easy regeneration by ion replacement using NaCl or mild alkaline elusion. Molecularly imprinted polymers (MIPs) provide another level of control by creating tailor-made binding cavities with complementary geometry and functionality to molecular structure of CM. The imprinted sites produce high selectivity (even in the presence of competing dyes or organic matter) due to their precise spatial and chemical recognition. However, diffusion limitations within the dense polymer matrix can reduce the adsorption kinetics, and template removal during synthesis can generate chemical waste, which raises environmental concerns.

Conducting polymers such as polyaniline (PANI) and poly-pyrrole (PPy) represent a special class due to their conjugated π-electron backbones. These materials adsorb CM primarily through π–π stacking between the aromatic rings of polymers and the azo-benzene groups of dyes, which are complemented by hydrogen bonding and electrostatic attraction in doped states.[122] Additionally, their redox-active nature allows them to partially reduce the azo bond ($-N{=}N-$), which integrates adsorption with catalytic detoxification. When incorporated into composites with carbon nanotubes, graphene oxide, or magnetic nanoparticles, conducting polymers exhibit enhanced surface area, better dispersibility, and facile recovery by magnetic separation. However, they are sensitive to oxidation,

undergo degradation over repeated cycles, and require acidic conditions to maintain their conductivity, which limits their practical wastewater application.

Hyper-crosslinked polymers (HCPs)[123] and covalent organic frameworks (COFs), due to their exceptionally high surface areas, hierarchical porosity, and rigid aromatic frameworks, show extraordinary adsorption performances through a combination of π–π interactions, hydrophobic effects, and size-selective pore filling. Their rigid skeletons provide stability under a wide range of pH and temperature, and functionalization (*e.g.*, with –NH_2, –OH, or quaternary groups) tailors them for anionic dye capture. Conjugated microporous polymers (CMPs) and COFs have a major advantage in that they can integrate adsorption with photocatalytic or photo-Fenton functionalities, which enable dye degradation within the adsorbent structure and thus reduce secondary waste generation.[124] However, their synthesis often requires toxic solvents, high temperatures, or costly monomers, which makes their large-scale production environmentally and economically challenging.

Ion-exchange resins and quaternized hydrogels demonstrate the highest practical removal efficiencies and regeneration potential, though their performance is limited by fouling and decreased selectivity in saline or multicomponent wastewater.[114] MIPs provide the best selectivity but suffer from slow kinetics and complex, often solvent-intensive synthesis. Conducting polymers excel in multifunctional adsorption–reduction behavior but degrade under prolonged exposure to oxidants or UV light. HCPs and COFs provide excellent capacity and structural stability but are costly and environmentally intensive to produce. Therefore, synthetic polymers outperform biological or inorganic adsorbents in capacity, selectivity, and reusability, while their environmental burden during synthesis and disposal remains a significant limitation.

The use of synthetic organic polymers for CM removal represents a double-edged sword. On the one hand, these materials provide durability, tunable functionality, high efficiency, and excellent regeneration, which are critical advantages in reducing operational waste and minimizing chemical consumption during treatment cycles. On the other hand, their synthesis pathways are resource- and energy-intensive, which involve petrochemical-based monomers and organic solvents that contribute to greenhouse gas emissions, residual toxicity, and solvent waste.[121] Furthermore, their non-biodegradability makes their post-use management challenging, as polymers can fragment into microplastics or leach monomeric residues, leading to secondary pollution. Also, their regeneration typically involves salt, base, or solvent washing, which generates secondary liquid waste requiring treatment, while thermal regeneration can cause polymer decomposition and release volatile organic compounds (VOCs).

Biological and natural polymer-based adsorbents are more environmentally benign but lack the robustness and adsorption precision of synthetic polymers. Inorganic materials provide structural stability but lack the fine-tuned selectivity achievable by synthetic polymers. Thus, the environmental challenge lies not in performance but in sustainable design. This involves adopting green polymerization methods, bio-derived monomers, and recyclable frameworks that reduce lifecycle impacts.

The adsorptive removal of CM by synthetic organic polymers illustrates the intersection of advanced materials chemistry and environmental engineering. These materials deliver precise, high-capacity, and regenerable adsorption through rational functionalization and structural optimization, outperforming natural systems under controlled conditions. However, their real-world sustainability depends on reducing their synthetic toxicity, improving their recyclability, and integrating hybrid strategies (coupling polymer adsorbents with photocatalytic, biological, or electrochemical regeneration) to achieve not only efficient dye removal but also environmental compatibility. Therefore, future development should focus on eco-designed polymers that balance high adsorption performance with minimal environmental footprint, which ensures both technological efficiency and ecological responsibility in CM remediation.

4.4 Photocatalytic materials

The photocatalytic degradation of CM by metal oxides and metal sulfides involves photon-induced electron–hole pair generation, interfacial charge transfer, and oxidative decomposition of the dye molecules into non-toxic or less toxic end products such as CO_2, H_2O, NO_3^-, and SO_4^{2-}. When a semiconductor photocatalyst is irradiated with light of energy equal to or greater than its band gap, electrons are excited from the valence band to the conduction band, leaving behind holes that participate in oxidation reactions. These charge carriers drive the formation of ROS, which attack the azo (–N≡N–) bond and aromatic moieties of CM, resulting in decolorization and stepwise mineralization. The main reactions include semiconductor excitation, water oxidation to $^{\bullet}OH$ by holes, and oxygen reduction to $^{\bullet}O_2^-$ by electrons, which together promote oxidative cleavage of the dye into smaller, less toxic fragments, as discussed in a previous section in detail.[125]

Metal oxides are the most widely used photocatalysts because of their chemical stability, strong oxidative potential, and environmental safety. Their wide band gaps (typically 3.0–3.2 eV) limit absorption to the UV region, but they can produce highly reactive hydroxyl radicals capable of complete mineralization of CM without forming harmful intermediates.[126] Modifications such as nonmetal doping, metal incorporation, and heterojunction construction are used to extend their light response into the visible region and reduce electron–hole recombination. In contrast, metal sulfides possess narrower band gaps (1.3–2.4 eV), which allow efficient utilization of visible light and enhanced solar activity. However, they are prone to photo-corrosion, where photogenerated holes oxidize S^{2-} to SO_4^{2-}, resulting in catalyst deactivation and potential metal ion leaching. This instability and possible release of toxic species such as Cd^{2+} and Cu^{2+} make sulfides less environmentally benign, despite their strong light absorption.

In terms of degradation mechanism, metal oxides typically generate hydroxyl radicals through water oxidation and proceed through oxidative pathways, leading to complete

mineralization. Conversely, metal sulfides mainly generate superoxide radicals owing to their less positive valence bands, which result in partial degradation or formation of aromatic intermediates unless stabilized through hybridization. To overcome these limitations, oxide–sulfide heterojunctions have been developed, where directional charge migration enhances the redox synergy and reduces recombination and photo-corrosion.[65] In these systems, the photogenerated electrons in the conduction band of the sulfide migrate to the oxide, while holes remain in the oxide valence band, maintaining a high redox potential and stability.[121]

The photocatalytic performance of both oxides and sulfides depends critically on several operational and structural parameters such as band-gap energy, band-edge positions, surface area, crystallinity, morphology, defect density, and heterojunction configuration.[127] Other factors such as light intensity, wavelength, catalyst dosage, pH, dissolved oxygen concentration, ionic strength, and presence of coexisting ions also significantly influence their degradation efficiency. For instance, at acidic pH, CM is more readily adsorbed on positively charged oxide surfaces, enhancing its degradation. Alternatively, at alkaline pH, repulsive interactions can suppress the reaction rates. Higher dissolved oxygen levels favor electron scavenging and $\cdot O_2^-$ formation, which reduce recombination losses, whereas competing anions such as Cl^- and HCO_3^- act as radical scavengers, which diminish the photocatalytic efficiency. Additionally, an excessive catalyst loading can cause light shielding or particle aggregation, which limits photon penetration and decreases the active site availability.

Metal oxides are more sustainable and stable, which produce minimal secondary pollution and allow easy recovery and reuse.[128] Their long-term performance remains high owing to their structural inertness and chemical resistance, which make them ideal for continuous water treatment applications. In contrast, metal sulfides (despite their superior visible-light absorption and higher quantum efficiency compared to metal oxides) suffer from poor durability and higher ecological risks owing to metal ion leaching and sulfide oxidation. Thus, the environmental impact of sulfide-based photocatalysts can only balance their photonic efficiency if they are properly immobilized or hybridized with protective oxide or carbonaceous layers.

Metal oxides achieve deeper mineralization and generate fewer toxic intermediates, while metal sulfides show faster decolorization but incomplete mineralization unless stabilized. The interplay among factors such as pH, light spectrum, oxygen availability, and heterojunction design can shift the degradation mechanism between direct hole oxidation (common in oxides) and ROS-mediated oxidation (dominant in sulfides). The overall conclusion is that oxide-based photocatalysts such as TiO_2 and ZnO remain the most environmentally safe and chemically stable materials for CM degradation, whereas sulfide-based catalysts such as CdS and MoS_2 provide enhanced solar utilization but demand careful stabilization to mitigate their environmental risks. The most efficient and sustainable strategy lies in hybrid systems that combine oxide and sulfide components or integrate carbon-based supporters, which enable efficient charge separation, broad-spectrum absorption,

and suppressed photocorrosion. Thus, optimizing physico-chemical parameters, material stability, and environmental compatibility is essential for achieving the high-performance and ecologically responsible photocatalytic degradation of CM in wastewater systems.

4.5 Biological materials for degradation of CM

The biological degradation of CM involves complex redox transformations governed by microbial enzymatic activity and environmental conditions.[111] This process typically occurs in two main phases as initial anaerobic reductive cleavage of the azo bond (–N═N–) followed by aerobic oxidative mineralization of the resulting aromatic amines. In the first phase, anaerobic or facultative microorganisms (particularly *Pseudomonas*, *Bacillus*, *Klebsiella*, and *Enterococcus* species) use azoreductase enzymes (NADH-dependent or flavin-based) to donate electrons to the azo bond, which split it into aromatic amines such as sulfanilic acid and naphthylamine derivatives. This reaction removes color rapidly but does not completely detoxify the effluent. The second, aerobic phase is critical for full degradation. Oxidative enzymes such as laccase, lignin peroxidase (LiP), and manganese peroxidase (MnP) break aromatic rings, generate quinones, and oxidize these intermediates into smaller organic acids that enter the tricarboxylic acid cycle and are finally mineralized to CO_2, H_2O, NO_3^-, and SO_4^{2-}. The efficiency and selectivity of each step are strongly influenced by the redox conditions (oxygen presence determines whether reduction or oxidation dominates) and co-substrate availability, pH, and temperature.

Bacterial systems are the most efficient for the first (reductive) step of CM degradation. Under oxygen-limited conditions, bacteria achieve high decolorization rates because azoreductases can access the azo bond readily when the dye is adsorbed on or near the cell surface. However, in environmental contexts, incomplete degradation can be problematic. Aromatic amines produced under anaerobic conditions are more toxic and mutagenic than the parent dye. Therefore, bacterial systems are effective for initial color removal but insufficient for full detoxification without an aerobic stage. In large-scale treatment plants, bacterial consortia within activated sludge show excellent performances but face limitations due to salinity, heavy metal interference, and unstable enzyme expression under fluctuating environmental conditions. The environmental implication of bacterial treatment is mixed. It reduces color and COD efficiently, while it risks producing toxic intermediates unless coupled with oxidative or photochemical polishing.

Fungal systems, particularly those based on white-rot fungi such as *Phanerochaete chrysosporium*, *Trametes versicolor*, and *Pleurotus ostreatus* excel at aerobic oxidation and detoxification of the amine intermediates. Fungal extracellular enzymes (especially laccases and peroxidases) have broad substrate ranges and catalyze one-electron oxidations that lead to ring cleavage and mineralization. Compared to bacteria, fungi degrade CM more completely, with higher total organic carbon (TOC) removal and reduced effluent toxicity. However, fungal

degradation is slower due to their lower growth rates and enzyme production, which depends on optimal nutrient balance, pH (4–6), and aeration. Environmentally, fungal systems are cleaner and produce less sludge, but their energy requirement for aeration and sensitivity to nutrient limitation can hinder large-scale continuous operation. The key advantage of fungal treatment lies in its ecological safety and complete mineralization, which balances slower kinetics when detoxification is the primary goal.[92]

Microalgae and cyanobacteria use a distinct mechanism involving biosorption, bioaccumulation, and photo-oxidation. Dyes such as CM are first adsorbed on algal cell walls (through electrostatic and hydrophobic interactions) and then undergo oxidative degradation assisted by oxygen and reactive oxygen species (ROS) produced during photosynthesis. Enzymes such as azoreductase and laccase-like oxidases also contribute intracellularly. Algal systems perform best in low-strength effluents under sunlight and provide dual benefits such as nutrient removal (N and P) and biomass generation for biofuel or fertilizer applications. However, they are slow at high dye concentrations due to light attenuation (self-shading), and their performance drops in cold or highly saline wastewater. Environmentally, algal systems are highly sustainable, which require no external carbon source or toxic reagents but are limited by climatic and light constraints. Their best use is as a tertiary polishing step after bacterial or fungal treatment to ensure final detoxification.

Enzyme-based systems, which utilize purified or immobilized enzymes (azoreductases, laccases, and peroxidases), facilitate precise and eco-friendly degradation of CM under mild conditions.[129] When immobilized on biopolymer supports such as chitosan, alginate, or silica, enzymes exhibit enhanced stability, reusability, and resistance to inhibitors. These systems allow direct oxidation or reduction of dye molecules without cell growth and prevent biomass accumulation.[130] However, they suffer from high enzyme production costs, deactivation in the presence of salts or surfactants, and diffusion limitations. Conversely, immobilized enzyme systems show excellent potential for clean, targeted removal of dyes in low-volume, high-value effluents. Environmentally, they minimize secondary pollution, but their large-scale sustainability depends on cost-effective enzyme recovery and regeneration.

Dead biomass and biosorbent-based materials, such as inactivated microbial cells, agricultural residues, and biochar, remove CM mainly through adsorption rather than true degradation. These biosorbents rapidly bind dyes due to surface functional groups (carboxyl, hydroxyl, and amine), enabling efficient color removal. However, the adsorbed dyes remain chemically intact, and desorption or disposal of the spent biosorbent poses a risk of secondary contamination. Although biosorption is low-cost and rapid, it is not a self-sustaining degradation method; it must be integrated with biological oxidation or advanced oxidation to achieve full detoxification. From an environmental perspective, biosorbents are advantageous due to their renewability and simplicity, but they merely transfer pollutants rather than eliminate them.

Bacterial systems provide the highest rate of color removal but risk incomplete degradation and formation of toxic intermediates. Fungal systems ensure deeper mineralization and detoxification but at slower kinetics. Algal systems contribute to sustainable polishing and nutrient recovery but are limited by light and temperature. Enzyme-based systems are cheap, selective, and produce little sludge but remain economically constrained. Biosorbent-based systems are the most affordable but least effective in long-term pollutant elimination. Thus, the environmental impact hierarchy can be summarized as: fungal = enzyme-based (lowest residual toxicity) > algal (moderate) > bacterial anaerobic (high toxicity risk) > biosorbent-only (secondary waste risk).

The parameters controlling the biological degradation of CM include redox potential (aerobic/anaerobic balance), pH (enzyme-specific activity windows), temperature (optimal for enzymes and growth typically 25–37 °C), co-substrate availability (electron donors such as glucose or acetate enhance reductive degradation), dye concentration, light intensity (for algal systems), and inhibitors (metal ions, surfactants, and salts). Environmental fluctuations in these parameters can shift the degradation pathways such as limited oxygen or high dye load can favor reductive azo cleavage (producing amines), while high oxygen and enzyme expression promote complete oxidation and mineralization. This interplay explains why real wastewater matrices often yield slower or incomplete degradation compared to lab-scale tests.

Biological degradation of CM represents a multifaceted, eco-friendly, and low-energy strategy, but one that requires careful process integration. Fast but incomplete bacterial reduction must be coupled with fungal or enzymatic oxidation for complete detoxification, while algal and biosorbent systems serve best in tertiary polishing. The environmental sustainability of biological methods is superior to chemical and physicochemical approaches, but their operational challenges (slow kinetics, sensitivity to conditions, and management of biological waste) must be addressed through process optimization, immobilization technologies, and hybrid systems combining biological and catalytic pathways.

A critical comparison between different materials is given in Table 3 which easily provides information on the advantages and limitations of each material for removal of CM.

4.6 Composite materials

The photocatalytic degradation and reduction of CM using hybrid composites that integrate metal nanoparticles, metal oxides, or metal sulfides with synthetic polymers,[121] biopolymers, carbonaceous materials,[104] metal–organic frameworks (MOFs), layered double hydroxides (LDHs), or zeolites[61] represents one of the most promising approaches for removing persistent azo dyes from wastewater. These composites exploit the synergistic coupling of multiple functionalities (adsorption, charge transfer, and redox catalysis) to overcome the individual limitations of pure materials. In these systems, the degradation or reduction of CM follows a multi-step mechanism involving dye adsorption on the composite surface, photoexcitation or

Table 3 Critical comparison among the materials used for the removal of CM from water

Type of materials	Examples	Role in combined system	Advantages	Limitations	Performances
Inorganic adsorbents	Layered double hydroxides (LDHs), zeolites, metal oxides (Fe_3O_4, Al_2O_3), silica	Provide surface adsorption and act as catalyst support	High thermal stability, tunable surface charge, structural robustness	Limited visible-light activity unless modified, lower adsorption capacity than carbon materials	Moderate-high adsorption, improved degradation when coupled with TiO_2/ZnO, stable over multiple cycles
Biological polymers	Cellulose derivatives, chitosan, alginate	High adsorption through –NH_2/–OH groups, support photocatalysts	Biodegradable, low-cost, abundant functional groups	Poor mechanical stability, swelling, limited long-term durability	High initial adsorption; enhanced degradation when crosslinked or combined with metal oxides
Photocatalytic materials	TiO_2, ZnO, g-C_3N_4, $BiVO_4$	ROS generation under light, oxidative degradation	Strong oxidative potential, mineralization capability	Electron–hole recombination, UV dependence (for some)	High degradation efficiency, improved when combined with adsorptive supports
Organic synthetic polymers	Polypyrrole (PPy), polyaniline (PANI), polymer resins	Conductive matrix, adsorption and electron mediator	Improved charge transfer, visible-light response, structural tunability	Possible photodegradation, synthesis can involve toxic reagents	Enhanced photocatalytic kinetics, good dye affinity, moderate recyclability
Biological materials (microbial/enzymatic)	Bacteria, fungi, laccase, peroxidases	Enzymatic reduction and adsorption	Eco-friendly, low energy demand	Slow kinetics, sensitive to pH/temperature, incomplete mineralization	Effective decolorization, limited mineralization without post-oxidation step

electron donation by the catalyst, charge carrier separation across heterointerfaces, and subsequent oxidative or reductive cleavage of the azo bonds (–N=N–). Upon illumination, photoinduced electrons reduce oxygen to superoxide radicals ($\cdot O_2^-$), while photogenerated holes oxidize water or hydroxide ions to hydroxyl radicals ($\cdot OH$), which initiate oxidative degradation. Simultaneously, in reductive environments or in the presence of reducing agents such as $NaBH_4$, the electrons from metal nanoparticles directly reduce the azo linkages to hydrazo intermediates, which lead to cleavage into aromatic amines that are later mineralized through secondary photocatalytic oxidation. The overall efficiency of this process depends critically on how effectively the composite material balances adsorption affinity, charge transfer rate, and redox potential.[106]

The integration of polymers or biopolymers such as chitosan, alginate, polyacrylamide, and polyaniline provides multiple advantages. These materials introduce reactive functional groups (–NH_2, –OH, –COOH, and –SO_3H) that enhance the electrostatic interaction and hydrogen bonding with the anionic sulfonate groups of CM, which significantly increase the adsorption preconcentration of the dye near the active sites. Moreover, polymer matrices act as capping and stabilizing agents, which prevent nanoparticle aggregation and leaching while maintaining high dispersion and accessibility to the catalytic sites. Biopolymers (being biodegradable and renewable) contribute to the environmental sustainability of the catalyst. However, their thermal and photochemical stability can be limited. Thus, their use is often optimized by crosslinking or hybridization with inorganic supporters. Carbonaceous materials such as GO, RGO, CNTs, and BC further improve the photocatalytic efficiency by acting as conductive

electron highways that accelerate interfacial charge transfer and suppress electron–hole recombination. Their π–π conjugation structures also facilitate dye adsorption through electron delocalization, which enhances visible-light utilization and the overall degradation kinetics.[109,124]

Metal oxides and metal sulfides incorporated into these matrices play distinct but complementary roles. Metal oxides show high oxidative potential and long-term chemical stability, which favor the deep mineralization of CM into CO_2, H_2O, and inorganic ions, although their wide band gaps limit visible-light absorption. Metal sulfides exhibit narrower band gaps and thus harvest visible light efficiently, but they are prone to photocorrosion and leaching, potentially introducing secondary pollution. By embedding these sulfides within conductive or polymeric matrices, the charge recombination and photocorrosion issues can be minimized through protective encapsulation and improved electron mobility.[104] Similarly, MOF-based composites contribute ultra-high surface areas, tunable pore structures, and the ability to anchor nanoparticles uniformly within their frameworks, which facilitate selective adsorption and catalytic reactions at the molecular scale. LDHs and zeolites provide additional benefits through their anion-exchange capacity and well-defined microporosity, which ensure enhanced adsorption of CM and efficient mass transfer. The synergistic interaction between these inorganic phases and organic supports produces a hierarchical composite with improved photophysical, structural, and chemical properties.

The environmental impact and comparative performance of these composite systems depend heavily on their composition, degradation pathways, and by-product formation.[121] Composites containing metal oxides or carbonaceous materials are

Table 4 Summary of nature of materials, removal process, optimized conditions, rate of removal, and removal percentage of CM

Nature of material	Material	Removal process	Rate of removal (min^{-1})	Optimized conditions	Removal percentage (%)	References
Biopolymer-metal oxide composite	Fe$_3$O$_4$@starch	Photocatalysis		30 °C, pH 7.0, 500 rpm, 250 W UV light	95	117
Inorganic-metal oxide composite	ZnO-surface modified activated carbon	Adsorption and photocatalysis	For adsorption $k_2 = 33.60 \times 10^{-3}$	pH 3, 30 °C, contact time = 60 min, photocatalyst = 0.09 g, 180 rpm, CM conc. = 25 mg L^{-1}	96	87
Semi-biopolymers	Carboxymethylcellulose-2-(dimethylamino)ethyl methacrylate-N-(3-(dimethylamino)propyl) methacrylamide	Adsorption		pH 2.1, 24 °C	98	116
Inorganic material	Porous silica	Adsorption	$k_1 = 0.124$, $k_2 = 1.142$	Temperature = 30 °C, pH 7, initial dye conc. = 45 mg L^{-1}	54	26
Metal-doped metal oxide	W-Cu-TiO$_2$	Photocatalysis, adsorption	For adsorption: $k_1 = 0.022$, $k_2 = 0.005$	pH 7, CM conc. of 50 mg L^{-1}	99	90
MOF-metal oxide composites	MIL-BiOI	Photocatalysis	$k_{app} = 0.002$ min^{-1}	pH 7, contact time of 75 min, photocatalyst content = 1.0 g L^{-1}	95	113
Inorganic-organic-metal oxide composites	Fe$_3$O$_4$@SiO$_2$/PAEDTC@ MIL-101	Photocatalysis	$k_{app} = 0.033$	pH 5, 36 W light, photocatalyst content = 0.5 g L^{-1}, CM conc. = 50 mg L^{-1}	100	128
Biological material	Natural diatomite	Adsorption	$k_1 = 0.043$ and $k_2 = 0.92$	pH 1, 20 °C, contact time of 30 min, conc. of CM = 50 mg L^{-1}, adsorbent content = 1 g L^{-1}		66
Carbonaceous material	Activated carbon	Absorption	$k_1 = 0.013$, $k_2 = 0.477$	pH 2, temperature of 45 °C, contact time of 60 min		24
Carbonaceous material	Biochar	Adsorption	$k_1 = 0.11$, $k_2 = 0.08$	pH 2, content of CM = 50 mg L^{-1}, 120 rpm, conc. of adsorbent = 0.12 g, contact time = 50 min	91	70
Metal-doped metal oxide	Cu$_{0.08}$Mn$_{0.02}$Fe$_{0.05}$Ce$_{0.85}$O$_2$	Photo-Fenton oxidation		pH 4, time = 20 min	95	20
Biological material	*Penicillium funiculosum*	Adsorption		pH 6.7, 160 rpm, 28 °C	100	130

generally regarded as environmentally safer because of their high recyclability, chemical stability, and low leaching potential. In contrast, sulfide-based composites show superior solar-light efficiency, but can release hazardous ions such as Cd^{2+} or Pb^{2+} upon prolonged exposure (especially under oxidative conditions), which raises toxicity concerns. Reduction-based systems that rely primarily on metal nanoparticles demonstrate rapid decolorization through efficient electron transfer but often produce partially reduced aromatic amines such as sulfanilic acid or 1-amino-2-naphthol, which are mutagenic and require secondary oxidation or biological degradation to ensure full mineralization. The most environmentally benign and effective composites are those that combine oxidative and reductive functions (often in the form of Z-scheme or S-scheme heterojunctions), where electrons and holes are spatially separated but maintain strong redox potentials, which enable the simultaneous reduction and oxidation of intermediate species.

The parameters controlling catalytic performance include both material properties and operational conditions. Material-specific factors encompass band gap energy, Fermi level alignment, crystal phase composition, particle size, surface area, pore structure, surface charge, and degree of interfacial contact between components. For instance, smaller nanoparticles increase the density of surface-active sites, while optimized band alignment between the semiconductor and conductive support enhances charge separation. Defect engineering (oxygen vacancies and sulfur vacancies) can extend the visible-light absorption and improve the carrier mobility, though excessive defects can increase the number of recombination centers. Operational parameters such as pH strongly influence the adsorption capacity (since CM is an anionic dye, acidic conditions generally enhance electrostatic attraction), while the presence of dissolved oxygen, ionic strength, light intensity, and catalyst loading determine the dominant reactive species and overall reaction rate. The surrounding environment (temperature, competing ions, and natural organic matter) also alters the kinetics and the selectivity of degradation pathways.

The hybridization of metal-based catalysts with polymers, biopolymers, and carbon frameworks significantly enhances their stability, reusability, and biocompatibility. Hence, these materials reduce nanoparticle leaching, minimizing the risk of secondary pollution. Compared with pure metal oxides or sulfides, composites provide more sustainable long-term performances, as their structural integrity and catalytic activity remain stable over multiple cycles. Furthermore, their broad-spectrum light absorption and increased radical generation lead to more complete degradation of CM, which minimizes the formation of toxic intermediates. However, critical challenges remain in scaling up these materials, managing synthesis costs, ensuring consistent recovery and reusability, and evaluating their ecotoxicological impacts comprehensively. Composite catalysts present a transformative advancement in CM remediation, which provides a path toward high-efficiency, solar-driven, and environmentally responsible dye removal. Their design and application balance activity, selectivity, and environmental safety across the entire lifecycle.

A summary of the materials used for the removal of carmoisine from water through photosynthesis/adsorption, along with their optimized conditions is provided in Table 4.

5 Characterization techniques

Removal of CM from water has been identified by various techniques such as spectral decolorization (UV-vis absorbance at λ_{max} of the dye) to confirm chromophore destruction,[131] intermediate identification (HPLC,[132] LC-MS, and GC-MS) to detect the presence of aromatic amines or ring-cleavage products, mineralization analysis (TOC/COD) to quantify organic carbon removal, inorganic analysis of end-products (IC for NO_3^- and SO_4^{2-}) to show true oxidation, catalyst/adsorbent characterization (XRD,[27] FTIR,[118] XPS,[133] and TEM) to evaluate structural changes, metal leaching experiments (ICP-MS) for nanocatalysts, and ecotoxicity/genotoxicity assays (Ames, *Daphnia*, algal growth, and Microtox) to evaluate environmental safety. The results obtained during these experiments can verify the efficiency of materials. Surface area and porosity are usually evaluated by Brunauer–Emmett–Teller (BET) analysis, with higher specific surface areas directly correlating to increased CM adsorption. Rapid loss of UV-vis signal alone only proves decolorization (not detoxification or mineralization).[131] Thus, robust studies must pair spectral kinetics with TOC/COD, LC-MS and toxicity tests. Reuse cycling, mass balance for catalysts, and leachate measurements are equally essential but under-reported.

Photocatalytic degradation by materials can be identified using different techniques. Pure metal oxides show reliable UV-vis decay of CM and moderate TOC removal under ideal illumination. However, pure oxides require UV or engineered visible-light modifications to be efficient under solar light. Metal-sulfide photocatalysts and plasmonic metal-decorated semiconductors exhibit faster visible-light decolorization because they harvest more photons, but many sulfides show poorer TOC removal and evidence of photo-corrosion or metal leaching (detected by ICP).[134] Composite photocatalysts are most frequently reported to exhibit the best combination of fast λ_{max} decay, higher apparent rate constants (k_{app}), and significantly improved TOC reductions. The analytical fingerprint is the faster disappearance of LC-MS intermediates and lower ecotoxicity after treatment. However, careful studies reveal that even high apparent rate constants can coincide with incomplete mineralization unless the catalyst preserves strong oxidative power. Hence, TOC and toxicity are the decisive metrics.

Adsorption capacity of adsorbents and product identification can also be monitored using different techniques. These results indicate the efficiency of the adsorbent for the removal of CM. Isotherm and kinetic analyses along with FTIR/XPS of spent adsorbents repeatedly indicate electrostatic binding, hydrogen bonding and π–π interactions as dominant mechanisms.[135] Adsorption studies show excellent color and concentration removal but negligible TOC reduction. The adsorbed concentration of CM by adsorbents can also be monitored using a UV-vis spectrophotometer, where a decline in the absorbance peak of CM is observed after its removal from a mixture by the

adsorbent. In this process, the pollutant is transferred to a solid. Therefore, regeneration tests (solvent or thermal) become a critical performance metric, where a decline in capacity across cycles and the nature of the desorption effluent determine whether adsorption is a viable long-term solution or simply a temporary containment step.

Catalytic reduction by metal nanoparticles and supported catalysts can also monitored using different techniques. UV-vis spectroscopy shows the near-instant disappearance of the λ_{max}, LC-MS shows the formation of aromatic amines almost immediately, while TOC barely changes during the reduction step. ICP-MS flags metal release if NPs are poorly stabilized. Practically, this technique is very helpful for monitoring rapid color removal or dye conversion into more biodegradable fragments, but not for stand-alone remediation. LC-MS and toxicity assays almost always demand follow-on oxidation/biological polishing to eliminate toxic amines. Bimetallic catalysts and well-engineered supports improve catalyst stability and lower leaching, resulting in improved reuse cycles and lower ICP values.

Morphological analysis through scanning electron microscopy (SEM)[118] and transmission electron microscopy (TEM)[27] is also routine, which allows the observation of particle size, porosity, and surface uniformity. In magnetic composites, such as NH_2–Fe_3O_4–WO_3, TEM revealed the uniform dispersion of the magnetic cores, while SEM coupled with energy-dispersive X-ray spectroscopy (EDX) confirmed the presence of functionalized amine groups and supported the observed stability during recycling. For magnetic composites, vibrating sample magnetometry (VSM) has been applied to confirm their strong magnetic response,[83] which ensures their easy recovery from treated water.

The performance order indicated by results is reduction > adsorption > photocatalysis in terms of visible color removal speed (reduction fastest, adsorption fast, and photocatalysis slower for TOC). For mineralization and toxicity reduction, photocatalysis generally outperforms the others when TOC and toxicity assays are considered.[31] Adsorption scores are high for robustness in complex matrices but low on final disposal/regeneration impacts. Catalytic reduction scores high on kinetics but low on final ecotoxic outcome unless followed by polishing. Regarding stability and reusability, carbon-supported photocatalysts and immobilized composites perform better than unsupported NPs or fragile enzyme systems.

Best-practice interpretation and integrated strategies (how to read technique results sensibly) are necessary. Do not judge a material only by % color removal or a single apparent rate constant (k_{app}). Prioritize studies that report such as UV-vis and LC-MS for intermediates, TOC/COD for mineralization, ecotoxicity/genotoxicity before and after treatment, catalyst/adsorbent reuse cycles and ICP-MS of leachate, and performance evaluations in realistic matrices (NOM and salts). The realistic treatment pathway supported by techniques is generally adsorption or fast reduction as pretreatment (rapid color and load reduction), followed by photocatalytic or biological polishing to ensure mineralization and detoxification. Composites that combine adsorption plus photocatalysis or reduction plus immediate oxidation show the most compelling and reproducible experimental outcomes.

Prioritize composites and immobilized catalysts that show repeatable TOC reduction and low metal leaching over multiple cycles, minimize formation of persistent amines (demonstrated by LC-MS disappearance and reduced ecotoxicity), work under visible light or sunlight (demonstrated quantum yields), and retain their adsorption capacity in the presence of NOM and salts (breakthrough tests). When evaluating new materials, a full analytical suite is required (UV-vis, LC-MS, TOC, toxicity,

Table 5 Materials, their components, typical characterization techniques used and factors affecting the removal of CM

Name of materials	Polymer components	Catalytic components	Characterization techniques	Factors	References
BiOI-M-MIL binary composite	Modified MIL-101	BiOI	UV-vis, XRD, SEM, TEM, BET, DRS, FTIR, XPS, TOC, LC-MS	Catalyst loading, irradiation time, light intensity, dye conc., pH of medium, effect of scavengers	113
ZnO-tyre composite (adsorbent/photocatalyst)	Carbon/ash derived from waste tyre	ZnO	UV-vis, BET, FE-SEM, EDX-map, XRD, FTIR	pH effect, contact time, adsorbent dose, initial conc., visible/UV light effect, ionic strength	108
Fe_3O_4@SiO_2/PAEDTC@MIL-101	SiO_2/PAEDTC@MIL-101	ZnO	TEM, SEM, XRD, BET, UV-vis, radical scavenger tests, LC-MS, TOC	Ultrasonic and light effect, pH, catalyst dose, effect of scavengers	128
Fe–Co–V nanostructure on zeolite	Zeolite	Fe–Co–V	XRD, FE-SEM, EDS, FTIR, TEM, BET, ICP zeta potential	pH effect, CM content, adsorbent dose, contact time, temperature effect, leaching effect	49
SiO_2-based stones (silica, zeolite, pumice, scoria)	Silica, zeolite, pumice	—	DLS, XRD, BET, XRF, FTIR	Effect of conc. of adsorbent and CM, pH of medium	26
Chitosan-polyvinyl alcohol	Chitosan, polyvinyl alcohol	—	SEM, FTIR, BET, VSM	pH, porosity, temperature	118
Cysteine-coated Fe_3O_4	Cysteine	Fe_3O_4	XRD, TEM, FTIR, VSM	Effect of pH, content of adsorbent, content of CM, and ionic strength	27

ICP, and reuse cycles), and only then can technique results be meaningfully compared and policy/engineering decisions be made.

A summary of the characterization techniques used for the identification of carmoisine removal from water through photosynthesis/adsorption is provided in Table 5.

6 Recycling

Recycling in CM remediation involves two main points. The regeneration and reuse of the material (adsorbent or photocatalyst) is the first and ensuring that degradation leads to non-toxic, mineralized products rather than secondary pollutants is the second. In adsorptive systems, regeneration is typically achieved through desorption processes. After saturation with CM, the adsorbent is separated (filtration or magnetic recovery), washed with an appropriate desorbing agent such as ethanol, NaOH, or dilute acid, and then rinsed and dried for reuse. The mechanism involves disruption of electrostatic attraction, hydrogen bonding, or π–π interactions between the dye molecules and surface functional groups. Thermal regeneration can also be applied, where controlled heating removes the adsorbed dye through decomposition. However, this method can damage surface porosity and increase energy consumption. Critically, efficient materials should retain at least 80% of their original adsorption capacity after multiple cycles (typically 4–6), and their structural stability must be confirmed through post-cycle characterization (FTIR, XRD, and SEM). Magnetic composites such as Fe_3O_4-based systems show superior recyclability because they enable rapid external magnetic separation, which minimizes material loss and operational cost.[64,86,136,137]

In photocatalytic degradation systems, the recycling process involves the recovery of the photocatalyst after treatment and its reuse without significant loss of activity. Generally, this process involves sedimentation or centrifugation (for suspended nanoparticles), washing with distilled water or ethanol to remove intermediates, drying, and reapplication under irradiation. Immobilized catalysts (coated on glass plates, membranes, or carbon supports) simplify this process, as they can be directly reused after washing without complex separation steps. Activity loss during cycles is commonly owing to surface fouling by intermediate by-products, partial photo-corrosion, or agglomeration of nanoparticles. Controlled calcination or light-assisted self-cleaning can restore activity by removing adsorbed residues. Critically, recyclability tests must include kinetic comparison (k_{app} values) over multiple cycles to verify long-term stability rather than relying solely on percentage removal. The formula used to determine the percentage efficiency of a photocatalyst is given in eqn (12).

$$\text{Percentage catalytic efficiency}(\%) = \frac{k_{app}(n\text{th cycle})}{k_{app}(1\text{st cycle})} \times 100 \quad (12)$$

A high percentage catalytic efficiency value indicates that there is no deterioration in the performance of the photocatalyst during recycling, whereas a low value indicates that the photocatalyst rapidly loses its activity during recycling.

Accordingly, a photocatalyst that maintains its performance during recycling is ideal for the degradation of CM because it reduces costs through its repeated reuse.

In ecosystems, besides the reuse of a material, its pathway for the complete mineralization of CM is important. Photocatalytic systems generate reactive oxygen species that cleave the azo bond (–N=N–), break aromatic rings, and convert intermediates into CO_2, H_2O, NO_3^-, and SO_4^{2-}, as discussed in the photocatalytic degradation mechanism. Monitoring total organic carbon (TOC) and identifying intermediate products through LC-MS or GC-MS are essential to confirm that toxic aromatic amines do not accumulate, as discussed in the characterization section. Without proper mineralization, partial degradation can pose greater ecological risk than the parent dye.

Therefore, a sustainable recycling process contains several steps, such as (i) efficient dye removal, (ii) easy separation of the material, (iii) mild regeneration without hazardous chemicals, (iv) minimal loss of structural integrity, and (v) confirmation of non-toxic end products. Future developments should focus on magnetically recoverable, solar-driven, self-regenerating hybrid composites synthesized through green routes, which enable scalable and circular wastewater treatment systems with reduced energy input and minimal secondary pollution.

7 Challenges and outlook

The field of adsorptive and photocatalytic removal of CM faces a set of interlinked scientific and practical challenges that must be tackled if laboratory advances are to translate into reliable, safe, and scalable treatments. A primary technical challenge is the frequent discrepancy between rapid color removal (decolorization) and true detoxification (mineralization). Many materials (especially reductive catalysts and simple adsorbents) achieve fast disappearance of the azo chromophore while producing aromatic amines (in the case of reductive catalysis) that are more toxic and persistent than the parent dye. A clear solution is the integration of strategies such as design treatment trains or multifunctional composites that combine adsorption or rapid reductive cleavage with a downstream oxidative-polishing stage (photocatalysis, AOP, or aerobic biodegradation). Therefore, future research should prioritize system-level demonstrations (bench-to-pilot) that quantify not only UV-vis kinetics but also TOC/COD removal, full speciation of intermediates by LC-MS, and ecotoxicity assays across sequential stages to prove net detoxification rather than cosmetic color removal.

Material stability, leaching and lifetime are other crucial constraints. Photocatalysts and metal nanoparticles suffer photo-corrosion, aggregation, or metal ion leaching under real wastewater conditions (salts, NOM, and variable pH), which undermine their reuse and raise secondary pollution risks. The remedy lies in rational materials engineering such as immobilizing active phases on robust supports (biochar, RGO, silica, and zeolites), which create core–shell or encapsulated architectures to block leaching, use alloying or single-atom dispersion to reduce total precious-metal loading, and exploit

magnetically recoverable platforms for easy retrieval. Future directions include the development of water-stable, low-leaching catalysts (*e.g.*, covalently anchored single-atom sites and MOF-derived carbons) and lifecycle-focused studies reporting metal leaching (ICP-MS) across repeated cycles, together with economic analyses for recovery and recycling.

Real-wastewater complexity is a persistent barrier in laboratory tests with single-solute model solutions, which overestimate performance because natural organic matter, inorganic anions (Cl^- and HCO_3^-), and co-contaminants quench radicals, compete for adsorption sites, or foul catalysts. Solutions include systematic matrix studies that simulate realistic conditions (high ionic strength, NOM, mixed dyes, and surfactants) and optimization of surface chemistry to favor the selective sorption/oxidation of CM. Future work should emphasize column and continuous-flow studies (not just batch), long-term fouling/regeneration cycles, and demonstration of robustness in pilot plants treating real effluents, with standardized reporting of breakthrough curves, mass balances, and effluent toxicity.

Regeneration and end-of-life management of adsorbents and photocatalysts represent another challenge with environmental consequences. Thermal/chemical regeneration can degrade materials and produce secondary waste, while disposal concentrates the pollutant in solid residues. Remedial strategies include designing regenerable adsorbents that desorb under mild conditions (salt, pH swing, and low-energy solvents), coupling adsorption to *in situ* oxidation that regenerates the sorbent (adsorptive–photocatalysis), and valorizing spent materials (*e.g.*, pyrolysis of loaded biochar to recover energy/metal). Future research should quantify the regeneration energy, capacity loss per cycle, and fate of concentrated residues, and develop circular protocols for catalyst/adsorbent recycling and metal recovery to reduce the lifecycle footprint.

Standardization of performance metrics is weak across the literature and impedes meaningful comparison. Many studies report only percent decolorization or k_{app} values under different light sources and catalyst doses. Following points should be need to improve the quality of research for CM remediation such as (i) initial and time-resolved UV-vis spectra, (ii) TOC/COD removal, (iii) LC-MS identification of intermediates and their temporal decline, (iv) ecotoxicity/genotoxicity assays pre- and post-treatment, (v) catalyst/adsorbent recyclability and metal leaching (ICP), (vi) experimental conditions (light spectrum, intensity, reactor geometry, O_2 level, pH, and ionic strength), and (vii) mass balance. As the future outlook, journals and reviewers should enforce these standards, and meta-analyses should aggregate data to reveal truly promising systems for scale-up.

Energy and economic viability are overlooked. Visible-light photocatalysts, sunlight-driven reactors, and low-energy regeneration methods are essential for practical deployment. Therefore, advances should target catalysts with high solar quantum efficiencies, low-cost abundant elements (Fe, Cu, and C-based materials) or minimal noble metal loadings (single-atom catalysts), and reactor geometries that maximize photon utilization at scale (flow-through, immobilized beds, and solar

concentrators). Techno-economic and life-cycle assessments must accompany laboratory reports to determine real-world feasibility. Future research should provide energy-per-mass-removed metrics and cost projections, which enable comparison with established treatments such as activated sludge or AOPs.

Mechanistic ambiguity limits rational design. Many studies fit kinetic models without probing elementary steps (adsorption *vs.* reaction and surface *vs.* bulk radical pathways). Deeper mechanistic interrogation using transient spectroscopy, radical scavenger studies with quantified scavenging rates, *in situ operando* spectroscopies, and modelling (DFT for adsorption energies and reaction barriers; kinetic-mass-transfer coupling) will enable predictive materials design. The outlook is a shift from empiricism to mechanism-driven optimization. Selectivity for CM over NOM is due to surface functional groups that drive specific electron/hole processes, and heterojunction engineering to preserve redox power while improving separation (preferring Z- or S-schemes when mineralization is the goal) are essential.

Health and ecotoxicological assessment of products must be central rather than peripheral. Routine inclusion of genotoxicity (Ames), acute toxicity (*Daphnia* and algae), and advanced bioassays for endocrine or mutagenic effects will reveal whether a proposed method actually lowers environmental risk. The solution is to make toxicity endpoints mandatory in efficacy studies and to develop standardized toxicity-to-TOC correlation frameworks. Future directions include coupling remediation studies with biodegradability tests (BOD/biodegradation indices) and tracking long-term ecological recovery in mesocosm experiments.

Reactor design and process integration are practical challenges. Lab reactors (stirred batch with artificial light) do not translate directly to field reactors. Solutions exist in modular design including immobilized catalyst panels, packed bed adsorbers with sequential AOP polishing, and integration into existing wastewater trains (pretreatment adsorption to catalytic reduction or photocatalysis to biological polishing). The future will see pilot demonstrations in textile effluent facilities with real performance reporting (mass throughput, sunlight *vs.* lamp energy, and maintenance cycles), which are essential for regulatory acceptance and industrial uptake. Pilot-scale and real wastewater validation must be prioritized over further small-scale batch optimization. Most studies are conducted in synthetic dye solutions under controlled laboratory conditions, which do not account for competing ions, organic matter, turbidity, or fluctuating pH in industrial effluents. Demonstrating performance in continuous-flow systems, fixed-bed reactors, or solar-driven pilot units will provide realistic evaluation of scalability, durability, and operational cost. Techno-economic analysis (TEA) and life-cycle assessment (LCA) should accompany pilot studies to determine commercial feasibility in future studies.

Sustainability in synthesis must be prioritized. Many high-performing materials rely on toxic solvents, harsh reagents, or energy-intensive processing. Green chemistry solutions (biogenic synthesis of metal nanoparticles, solvent-free polymerization, low-temperature hydrothermal routes, and use of biomass-derived carbon supporters) must be scaled and

benchmarked. The future trajectory should favor materials whose upstream environmental impacts are lower than the benefits they deliver, as verified through cradle-to-grave life-cycle assessment. This field should shift from maximizing decolorization to ensuring complete mineralization and toxicity suppression, integrating mechanistic studies with ecotoxicological evaluation. By prioritizing standardization, real-world validation, and environmentally responsible materials design, future research can transition from laboratory innovation to sustainable industrial application.

Combined processes such as adsorption-biological degradation and adsorption-chemical reduction present capable but complex strategies for dye removal, and thus their practical implementation faces several scientific and engineering challenges that must be critically addressed. In adsorption-biological degradation systems, adsorption acts as a pre-concentration step, which capture dye molecules onto a solid support, while microorganisms or enzymes subsequently degrade the adsorbed pollutants. The major challenge lies in maintaining biological activity after adsorption. High local dye concentrations on the surface can inhibit microbial metabolism or enzyme function due to toxicity. Additionally, environmental factors such as pH, temperature, oxygen availability, and nutrient supply strongly influence the biodegradation efficiency. Another limitation is incomplete mineralization. Azo dyes can be reduced to aromatic amines under anaerobic conditions, which are potentially more toxic and persistent. Therefore, ensuring sequential aerobic post-treatment or integrating oxidative steps is critical to prevent the accumulation of hazardous intermediates. From a stability perspective, biofouling, microbial washout, and limited long-term operational durability also restrict scalability. Similarly, in adsorption-chemical reduction systems, the adsorbent first captures dye molecules, after which a reducing agent (*e.g.*, NaBH$_4$, zero-valent metals, and catalytic nanoparticles) facilitates electron transfer to cleave azo bonds. While this approach can achieve rapid decolorization, it generates aromatic amine intermediates rather than complete mineralization. A key challenge is controlling reductive pathways to avoid secondary contamination. Moreover, the use of chemical reductants introduces cost, safety, and waste management concerns. Catalyst deactivation, nanoparticle aggregation, and leaching of metal ions further limit recyclability and environmental compatibility. Therefore, while adsorption improves contact efficiency and accelerates reduction kinetics, the sustainability of the process depends on reagent consumption, by-product toxicity, and catalyst stability.

These challenges indicate that the future of CM remediation lies in integrated, mechanism-informed, lifecycle-aware approaches. Develop hybrid materials and integrated systems that enable rapid pollutant capture followed by fast mineralization. Emphasize material stability with negligible leaching, adopt standardized reporting and toxicity evaluation protocols, and demonstrate techno-economic viability at pilot scale. Addressing these requirements will help translate promising laboratory materials into practical, safe, and sustainable solutions for treating dye-contaminated water.

8 Conclusion and future directions

The comprehensive study of adsorptive and photocatalytic removal of CM highlights significant progress in pollutant remediation, but critical challenges persist in translating laboratory-scale results into practical, sustainable applications. Various materials such as metal oxides, metal sulfides, carbon-based composites, biopolymers, and metal–organic frameworks have shown high degradation and adsorption efficiencies due to their diverse surface chemistries, active sites, and electronic properties. However, most studies are confined to controlled laboratory conditions that do not accurately mimic real waste-water environments containing competing ions, fluctuating pH, and organic matter. This limitation results in overstated performance outcomes that fail to represent real-world efficiency. Additionally, inconsistencies in testing parameters such as catalyst dosage, light intensity, and pollutant concentration complicate the comparison of results across studies, while the incomplete mineralization of CM and formation of toxic intermediates remain underreported. These gaps highlight the need for standardized testing protocols and deeper mechanistic understanding supported by spectroscopic and computational investigations to identify true reaction pathways and stability factors governing degradation.

The synergistic use of hybrid composites (especially those integrating metal oxides or sulfides with polymers, carbonaceous matrices, or biopolymers) has emerged as a promising strategy to overcome the limitations of pure materials. These composites combine adsorption and photocatalytic functionalities, which enable dye pre-concentration followed by efficient photo-degradation through enhanced charge separation and surface reactivity. Hybrids exhibit higher activity and recyclability compared to their pristine counterparts, owing to their improved porosity, lower electron–hole recombination, and tunable surface charge. In contrast, these systems face drawbacks including complex synthesis procedures, high production costs, and potential nanoparticle leaching, which could pose secondary environmental risks. To mitigate these, future work must focus on green synthesis routes, cost-effective raw materials, and structural stability over multiple reuse cycles, which ensure long-term operational safety and environmental compatibility.

Future opportunities in these combined systems lie in rational materials engineering and process integration. For adsorption-biological systems, immobilizing enzymes or microbial consortia onto porous, biocompatible supports can enhance their stability and resistance to toxicity. Designing sequential anaerobic–aerobic reactors can ensure azo bond cleavage followed by oxidative mineralization of aromatic amines. In adsorption-chemical reduction systems, replacing hazardous reductants with green electron donors (*e.g.*, plant-derived reducing agents or electrochemical reduction) can improve sustainability. Magnetic or immobilized catalysts can enhance recovery and minimize metal leaching. Ultimately, integrating adsorption with complementary degradation pathways (quantitatively assessing toxicity, energy demand, and material longevity) offers a promising route toward efficient,

scalable, and environmentally responsible dye remediation technologies.

The environmental implications of these remediation processes are profound, as poorly optimized systems may generate partially degraded aromatic intermediates that are more toxic than the parent dye. Therefore, research should prioritize the complete mineralization of CM to CO_2, H_2O, and non-toxic ions rather than focusing solely on color removal efficiency. Moreover, the shift toward visible-light-active catalysts and solar-driven systems is essential to minimize energy consumption and environmental impact. In parallel, the integration of adsorption and photocatalysis into hybrid "adsorptive–photocatalytic" processes can enhance efficiency by capturing dyes on the surface before photodegradation and show higher overall pollutant removal. Nevertheless, translating these approaches to large-scale treatment demands optimization of catalyst immobilization, reactor design, and fluid dynamics to enable continuous-flow operations with minimal secondary pollution.

Future directions in this field must include the development of standardized evaluation metrics such as total organic carbon (TOC) reduction, toxicity index, and quantum efficiency, which can provide more meaningful measures of environmental safety and catalytic performance. Real wastewater validation and long-term cycling experiments should replace batch testing in deionized water to assess durability and scalability under realistic conditions. Additionally, *in situ* spectroscopic characterization and density functional theory (DFT) simulations should be employed to correlate electronic structure modifications with photocatalytic performance, which enable the rational design of next-generation catalysts. The incorporation of green and circular economy principles (using biomass-derived carbons, biodegradable polymers, and waste-derived metal sources) will further reduce the environmental footprint of catalyst synthesis. The future of CM removal lies in developing multifunctional, solar-driven, and eco-friendly hybrid materials that ensure complete degradation, recyclability, and low energy input. The convergence of materials innovation, environmental science, and engineering optimization will ultimately determine the transition of these systems from laboratory experiments to scalable, sustainable wastewater treatment technologies.

TEM	Transmission electron microscopy
EDX	X-ray spectroscopy
E_g	Energy band gap
VSM	Vibrating sample magnetometry
VOCs	Volatile organic compounds
LC-MS	Liquid chromatography-mass spectrometry
ICP	Inductively coupled plasma
AOPs	Advanced oxidation processes
CMPs	Conjugated microporous polymers
COFs	Covalent organic frameworks
MIPs	Molecularly imprinted polymers
HCPs	Hyper-crosslinked polymers
SBA-15	Santa barbara amorphous-15
MPS	Mesoporous silica
MOFs	Metal–organic frameworks
CNT	Carbon nanotube
PANI	Polyaniline
PPy	Polypyrrole
MCM-41	Mobil composition of matter no. 41
MNPs	Metal nanoparticles
CS	Chitosan
AC	Activated carbon
LDH	Layered double hydroxides
DMF	Dimethylformamide
DMSO	Dimethyl sulfoxide
PZC	Point of zero charge
SPR	Surface plasmon resonance
RGO	Reduced graphene oxide
GO	Graphene oxide
LC-MS	Liquid chromatography-mass spectrometry
ICP-MS	Inductively coupled plasma-mass spectrometry
BC	Biochar
HC	Hydrochar
PSO	Pseudo-second-order
PFO	Pseudo-first-order
COD	Chemical oxygen demand
NOM	Natural organic matter
ZL	Zeolite
LiP	Lignin peroxidase
MnP	Manganese peroxidase

Conflicts of interest

There is no conflicts of interest.

List of abbreviations

MOx	Metal oxide
Carmoisine	CM
NPs	Nanoparticles
ROS	Reactive oxygen species
CB	Conduction band
VB	Valence band
DFT	Persulfate density functional theory
TOC	Total organic carbon
SEM	Scanning electron microscopy

Data availability

No primary research results, software or codes have been included, and no new data were generated or analysed as part of this review.

Acknowledgements

References

1 M. K. Sadannavar, A. Periyasamy, S. R. Islam, F. Shafiq, X. Dong and T. Zhao, Natural Dyeing and Antimicrobial Functionalization of Wool Fabrics Dyed with Chinese

Dragon Fruit Extract to Enhance Sustainable Textiles, *Sustainability*, 2024, **16**, 6832, DOI: 10.3390/SU16166832.

2 D. M. Cassingham and G. Roentgen, Investigation into the eco-friendly, simultaneous tanning and reactive dyeing of leather, *Color. Technol.*, 2025, **142**, 102–118, DOI: 10.1111/COTE.12818.

3 H. E. H. Ahmed, Z. P. Gumus and M. Soylak, Switchable solvent-based liquid phase microextraction of Sudan dyes in food and water samples with HPLC-DAD, *J. Food Compos. Anal.*, 2025, **139**, 107099, DOI: 10.1016/J.JFCA.2024.107099.

4 S. Adeel, S. Abrar, M. Ozomay, F. Rehman, M. Hussaan and F. Batool, Evolving role of plant pigments in the cosmetic industry, in.*Renewable Dyes and Pigments*, 2024, pp. 307–319, DOI: 10.1016/B978-0-443-15213-9.00014-4.

5 Pritee, S. Sharma and S. Thakur, Facile Green One-Pot Synthesis of Pyrimidine Based Hydroxy Azo-Polymer for Selective Adsorption of Cationic Dyes, *Chem. Afr.*, 2025, **8**(3), 1101–1114, DOI: 10.1007/S42250-024-01169-W.

6 S. Premcheska, M. Lederer, S. Mohanty, A. Alici, A. G. Skirtach and A. M. Kaczmarek, Novel Type of Non-Toxic, Degradable, Luminescent Ratiometric Thermometers Based on Dyes Embedded in Disulfide-Bridged Periodic Mesoporous Organosilica Particles, *Adv. Opt. Mater.*, 2024, **12**, 2401026, DOI: 10.1002/ADOM.202401026.

7 H. Ramesh and A. K. Bhuyan, Food Colorants Acid Yellow 23, Azorubine, and Acid Red 18 Cause Aggregation and Fibrillation of Proteins, *ACS Food Sci. Technol.*, 2024, **4**, 963–974, DOI: 10.1021/ACSFOODSCITECH.3C00707.

8 M. N. Mustafa, F. Hussain, M. Hussain, R. Hussain, K. Ayub, S. Muhammad, M. U. Khan, M. Ehsan and M. Adnan, Elucidating the Potential of Nonlinear Optical Behavior of Azo Dyes for Advanced Laser-Based Technologies, *Adv. Theory Simul.*, 2025, **8**, 2401202, DOI: 10.1002/ADTS.202401202.

9 P. Palma, M. Godoy and R. Calderón, Simultaneous determination of 11 water-soluble synthetic colorants in foods consumed in Chile by high-performance liquid chromatography with diode Array detection, *Food Chem.*, 2024, **460**, 140553, DOI: 10.1016/J.FOODCHEM.2024.140553.

10 K. Ma, Y. Zhang and T. Wu, Accurate Determination of 24 Water-Soluble Synthetic Colorants in Premade Cocktail Using Ultra-Performance Liquid Chromatography with Diode Array Detection, *Beverages*, 2025, **11**, 91, DOI: 10.3390/BEVERAGES11030091/S1.

11 K. Ramamurthy, P. S. Priya, R. Murugan and J. Arockiaraj, Hues of risk: investigating genotoxicity and environmental impacts of azo textile dyes, *Environ. Sci. Pollut. Res.*, 2024, **31**(23), 33190–33211, DOI: 10.1007/S11356-024-33444-1.

12 B. Taheri, M. S. Zakerhamidi, A. N. Shamkhali, R. Kian and A. A. Sadeghan, Solvent polarity effect on photophysical properties of some aromatic azo dyes with focus on tautomeric and toxicity competition, *Sci. Rep.*, 2025, **15**(1), 1–21, DOI: 10.1038/s41598-025-00001-w.

13 T. Li, L. Wei, Y. Fang, Y. Cui, X. Wang and Y. Li, Risk identification of human health, ecotoxicity, and degradation products of azo dyes: development of a priority control list, *Environ. Pollut.*, 2025, **386**, 127180, DOI: 10.1016/J.ENVPOL.2025.127180.

14 S. G. Kara, D. Yuzbasioglu, E. Avuloglu-Yilmaz and F. Unal, Do the azo food colorings carmoisine and ponceau 4R have a genotoxic potential?, *Toxicol. Res.*, 2025, **14**, tfaf033, DOI: 10.1093/TOXRES/TFAF033.

15 E. Toraman, Biochemical and molecular evaluation of oxidative stress and mitochondrial damage in fruit fly exposed to carmoisine, *Mol. Biol. Rep.*, 2024, **51**(1), 1–9, DOI: 10.1007/S11033-024-09616-0.

16 T. Pius Monsi, O. Amba Ollor, N. Concilia, T. Pius and A. Ollor, Assessment of Modulatory Effect of Some Synthetic Food Dyes (Carmoisine and Tartrazine) on Gut Microbiota of Albino Rats, *Int. J. Microbiol. Res.*, 2025, **35**, 15–24, DOI: 10.9734/mrji/2025/v35i31547.

17 B. Z. Shok, L. Amagon, N. N. Wannang, K. I. Amagon, E. E. Okpalaeke, J. G. Gotep and I. L. Elisha, Effects of selected food dyes on the reproductive system of male albino rats, *West Afr. J. Pharm.*, 2024, **35**, 92–100, DOI: 10.60787/WAJP.VOL35NO2.358.

18 T. C. M. Segato, E. L. A. Caetano, R. D. B. Mott, N. L. D. A. Ibanez, C. D. A. C. Frattes, C. D. A. Lima, M. R. Alves, V. C. Santos-Ebinuma and D. Grotto, A 90-day oral toxicity study evaluation of azaphilone derived from Talaromyces amestolkiae: A natural food colorant, *Food Chem. Toxicol.*, 2025, **200**, 115394, DOI: 10.1016/J.FCT.2025.115394.

19 I. M. Iloamaeke, N. J. Nnaji, E. C. Okpala, A. N. Eboatu and T. U. Onuegbu, Mercenaria mercenaria shell: Coagulation-flocculation studies on colour removal by response surface methodology and nephlometric kinetics of an industrial effluent, *J. Environ. Chem. Eng.*, 2021, **9**, 105715, DOI: 10.1016/J.JECE.2021.105715.

20 I. V. Zagaynov, I. V. Shelepin and E. Y. Liberman, Optimization of ceria catalysts for the removal of organic pollutants, *Mater. Lett.*, 2025, **401**, 139269, DOI: 10.1016/J.MATLET.2025.139269.

21 G. M. D. de Vasconcelos, I. K. Della-Flora, M. Kelbert, L. M. de Andrade, D. de Oliveira, S. M. D. A. Guelli Ulson de Souza, A. A. Ulson de Souza and C. J. de Andrade, Screening of Azo-Dye-Degrading Bacteria from Textile Industry Wastewater-Activated Sludge, *Eng*, 2024, **5**, 116–132, DOI: 10.3390/ENG5010008.

22 K. L. Chuang, Y. C. Lin, F. H. Hsu, C. K. Lin, M. C. Ferrari and H. H. Tseng, Design of high antifouling pH-responsive membrane for anionic dye filtration under alkaline conditions, *J. Membr. Sci.*, 2025, **727**, 124055, DOI: 10.1016/J.MEMSCI.2025.124055.

23 F. Erek, A comparative study on magnetic solid phase extraction and magnetic colloidal gel based-dispersive solid phase extraction methods for preconcentration of carmoisine (E 122) in food samples, *J. Food Compos. Anal.*, 2025, **139**, 107091, DOI: 10.1016/J.JFCA.2024.107091.

24 S. Chaudhary, M. Chaudhary, V. Tyagi, S. Chaubey, Suhas, V. Gupta, I. Pestana da Paixão Cansado and J. Ahmed, Sustainable Production of Porous Activated Carbon from Hydrothermally Carbonized Jamoya Fruit Seeds and Its Potential for Adsorbing the Azo Dye Carmoisine B, *Processes*, 2025, **13**, 385, DOI: 10.3390/PR13020385.

25 B. Sanay, R. Bozbay, S. Ciftbudak, Z. Ulker, S. Teke, Z. Akyol, E. P. Ozdemir and N. Orakdogen, Epoxy-Functional (Alkyl) methacrylate-Based Hybrids Reinforced with Layered Silicate Montmorillonite: From Mechanistic Study to Sustainable Wastewater Treatment, *Gels*, 2025, **11**, 803, DOI: 10.3390/GELS11100803/S1.

26 P. Bahman, T. Bagheri Lotfabad, A. Heydarinasab and S. Yaghmaei, Adsorption of carmoisine and malachite green on silicon dioxide-based stones nanosized by ball milling, *Adv. Environ. Sci. Technol.*, 2024, **10**, 142–159, DOI: 10.22104/AET.2024.6740.1840.

27 S. Nikzad Shalkouhi, H. Kefayati and S. Shariati, Cysteine-coated Magnetite Nanoparticles for the Removal of Carmoisine Edible Dye from Aqueous Medium, *Comb. Chem. High Throughput Screen.*, 2023, **27**, 2861–2870, DOI: 10.2174/0113862073259873231018081113/CITE/REFWORKS.

28 S. Badiger, K. Kaur and P. V. Nidheesh, Iron-modified coconut shell biochar-activated peroxymonosulfate for acetaminophen degradation and microbial inactivation in sewage, *Environ. Sci.*, 2025, **11**, 3161–3179, DOI: 10.1039/D5EW00800J.

29 I. El Mrabet, B. L. C. Santos, K. Tanji, E. Rombi, P. Parpot, A. M. Fonseca, H. Zaitan and I. C. Neves, Bimetallic-zeolite nanomaterials as catalysts for degradation of azorubine dye *via* Fenton-like oxidation, *J. Water Proc. Eng.*, 2025, **71**, 107341, DOI: 10.1016/J.JWPE.2025.107341.

30 M. A. Akl, A. A. H. Fahim and E. S. R. H. El-Gharkawy, Novel dihydroxybenzohydrazide grafted deoxycellulose for efficient removal of anionic food colorants and hexavalent chromium from wastewater, *Sci. Rep.*, 2025, **15**(1), 1–27, DOI: 10.1038/s41598-025-14609-5.

31 C. D. E. C. Chan, L. F. Alsalem, M. Almalki, I. Bozhinovska, J. S. Hayward, S. S. N. Williams and J. K. Bartley, Microwave-Assisted Degradation of Azo Dyes Using NiO Catalysts, *Catalysts*, 2025, **15**, 702, DOI: 10.3390/CATAL15080702.

32 C. Yida, Y. Qiaoling, L. Chengbao, Z. Leizhi, C. Feng, Q. Junchao, Q. Yongbin, M. Xianrong and C. Zhigang, Synthesis of CuOQDs/g-C3N4/C Composites *via* Stem Template Induction and their Photocatalytic Properties, *J. Water Proc. Eng.*, 2024, **4**, E2665976X334005, DOI: 10.2174/012665976X334005241021062812.

33 B. Balachandran and P. C. Sabumon, A comprehensive review on biodegradation of azo dye mixtures, metabolite profiling with health implications and removal strategies, *J. Hazard. Mater. Adv.*, 2025, **19**, 100834, DOI: 10.1016/j.hazadv.2025.100834.

34 A. B. Isaev, N. S. Shabanov, A. G. Magomedova, P. V. Nidheesh and M. A. Oturan, Electrochemical oxidation of azo dyes in water: a review, *Environ. Chem. Lett.*, 2023, **21**(5), 2863–2911, DOI: 10.1007/s10311-023-01610-5.

35 F. T. Geldasa, M. A. Kebede, M. W. Shura and F. G. Hone, Experimental and computational study of metal oxide nanoparticles for the photocatalytic degradation of organic pollutants: a review, *RSC Adv.*, 2023, **13**, 18404–18442, DOI: 10.1039/d3ra01505j.

36 A. Chaturvedi, B. N. Rai, R. S. Singh and R. P. Jaiswal, A comprehensive review on the integration of advanced oxidation processes with biodegradation for the treatment of textile wastewater containing azo dyes, *Rev. Chem. Eng.*, 2022, **38**, 617–639, DOI: 10.1515/revce-2020-0010.

37 M. Alfakeer, R. N. Felaly, S. S. Al-Juaid, D. F. Seyam, E. M. Mabrouk and M. Abdallah, Synthesis and cyclic voltammetric studies of azo dye compounds derived from 1,5-dihydroxynaphthalene and their application as corrosion inhibitors for carbon steel in hydrochloric acid solution, *Int. J. Electrochem. Sci.*, 2025, **20**, 100892, DOI: 10.1016/J.IJOES.2024.100892.

38 M. Iammarino, A. Mentana, D. Centonze, C. Palermo, M. Mangiacotti and A. E. Chiaravalle, Simultaneous determination of twelve dyes in meat products: Development and validation of an analytical method based on HPLC-UV-diode array detection, *Food Chem.*, 2019, **285**, 1–9, DOI: 10.1016/J.FOODCHEM.2019.01.133.

39 P. Koli and A. Charan, Photo-stability of Carmoisine 'A' dye in the presence of Lactic acid-Cocamidopropylbetaine surfactant-NaOH: A spectral study, *Opt. Mater.*, 2024, **155**, 115918, DOI: 10.1016/J.OPTMAT.2024.115918.

40 F. Uzcan, E. Yilmaz and M. Soylak, Development and Factorial Experimental Design Optimization of Deep Eutectic Solvent-Based Microextraction of Carmoisine (E122) in Candy and Water Samples, *Anal. Lett.*, 2023, **56**, 2172–2181, DOI: 10.1080/00032719.2022.2158194.

41 P. Barciela, A. Perez-Vazquez and M. A. Prieto, Azo dyes in the food industry: Features, classification, toxicity, alternatives, and regulation, *Food Chem. Toxicol.*, 2023, **178**, 113935, DOI: 10.1016/J.FCT.2023.113935.

42 I. Elekima, A. O. Nworgu and A. E. Okwuchi, Acute Assessment of Azorubine Exposure on Testosterone, Progesterone, Estradiol, Follicle Stimulating Hormone, Luteinizing Hormone, and Prolactin in Male and Female Albino Rats, *Asian J. Res. Rep. Endocrinol.*, 2025, **8**, 57–68, DOI: 10.9734/AJRRE/2025/V8I1107.

43 M. S. Khan, M. T. Rehman, G. M. Shaik, A. Mohammed Alamri, M. F. AlAjmi, M. Arshad and M. S. Alokail, Aggregation and cytotoxicity of food additive dye (Azorubine)-albumin adducts: a multi-spectroscopic, microscopic and computational analysis, *J. Biomol. Struct. Dyn.*, 2025, **43**, 946–956, DOI: 10.1080/07391102.2023.2289046.

44 M. A. Guerrero-Rubio, S. Hernández-García, F. García-Carmona and F. Gandía-Herrero, Consumption of commonly used artificial food dyes increases activity and oxidative stress in the animal model Caenorhabditis elegans, *Food Res. Int.*, 2023, **169**, 112925, DOI: 10.1016/J.FOODRES.2023.112925.

45 A. T. Bişgin, A. Ö. Altunay and A. Elik, Quadratic Box-Behnken-designed microextraction approach using organic acid-assisted magnetic deep eutectic solvent for the spectrophotometric determination of carmoisine (E122) in foodstuffs, soft drinks, and cosmetic products, *Sustainable Chem. Pharm.*, 2025, **46**, 102110, DOI: 10.1016/J.SCP.2025.102110.

46 S. Dutta, N. S. Khan, K. Bose and N. K. Poddar, A comparative *in silico* study to detect the effect of food-additives on metabolic protein and its perturbations compensated by osmolytes, *Int. J. Biol. Macromol.*, 2022, **216**, 179–192, DOI: 10.1016/J.IJBIOMAC.2022.06.152.

47 H. H. Alsharief, N. M. Alatawi, A. M. Al-bonayan, S. H. Alrefaee, F. A. Saad, M. G. El-Desouky and A. A. El-Bindary, Adsorption of Azorubine E122 dye *via* Na-mordenite with tryptophan composite: batch adsorption, Box–Behnken design optimisation and antibacterial activity, *Environ. Technol.*, 2024, **45**, 3496–3515, DOI: 10.1080/09593330.2023.2219399.

48 Q. Salamat and M. Soylak, Novel magnetic deep eutectic solvent/Zn-MOF composite for extraction of Carmoisine from water and food samples, *J. Food Compos. Anal.*, 2024, **128**, 105997, DOI: 10.1016/J.JFCA.2024.105997.

49 M. Kazem and K. Nasin, Adsorptive Removal of Carmoisine and Erythrosine from Aqueous Media by Fe-Co-V Nanostructure Supported on Zeolite, *Int. J. Chem. Chem. Eng.*, 2024, **43**, 3596–3609.

50 B. E. K. S. Puneeth, Carmoisine A Catalytic Film on The Surface of a One-Use Electrode for the Detection of Hazardous Culinary Ingredients Tartrazine in the Existence of Vanillin, *Anal. Bioanal. Electrochem.*, 2025, **17**, 162–172, DOI: 10.22034/ABEC.2025.721574.

51 S. Saipriya, J. G. Manjunatha, K. Bhimaraya, N. Ataollahi, S. A. Aldossari and E. S. D'Souza, Electrochemical development of alanine-modified carbon paste sensor for voltammetric detection of carmoisine in the presence of indigo carmine, *Monatsh. Chem.*, 2025, **156**(4), 407–418, DOI: 10.1007/S00706-025-03310-Y.

52 K. R. Shashank, J. G. Manjunatha, K. Bhimaraya, D. K. Ravishankar, V. Nandakumar, A. S. Alur, N. Sreeharsha and T. C. Canevari, An Electrochemically Polymerized Glycine-Modified Carbon Paste Sensor for the Analysis of Carmoisine in the Presence of Environmentally Significant Dyes, *J. Electron. Mater.*, 2025, **54**(11), 9811–9825, DOI: 10.1007/S11664-025-12359-8.

53 S. S. Nasrollahi, Y. Yamini and A. Mani-Varnosfaderani, A green approach for in-tube solid phase microextraction of acidic red dyes from juice samples using chitosan/poly vinyl alcohol electrospun nanofibers, *J. Food Compos. Anal.*, 2022, **106**, 104339, DOI: 10.1016/J.JFCA.2021.104339.

54 D. M. M. Elawady, E. R. H. El-Gharkawy and M. A. Akl, Design, Spectroscopic Analysis, DFT Calculations and Biosorption Evaluation of Pristine Ostrich Bone Biosorbent towards efficient removal of hexavalent chromium and flavoring and coloring agents from wastewater in single and multi-contaminant systems,

Egypt, *J. Chem.*, 2025, **68**, 565–593, DOI: 10.21608/EJCHEM.2025.358578.11278.

55 S. Ahmadi, M. Hasanzadeh and Z. Ghasempour, Sub-micro electrochemical recognition of carmoisine, sunset yellow, and tartrazine in fruit juices using P(β-CD/Arg)/CysA-AuNPs/AuE, *Food Chem.*, 2023, **402**, 134501, DOI: 10.1016/J.FOODCHEM.2022.134501.

56 A. Mirabi and B. Norouzi, Preparation of mesoporous silica SBA-15 modified by CTAB for extraction, preconcentration and determination of trace amounts of carmoisine in food samples, *J. Porous Mater.*, 2025, **2025**, 1–14, DOI: 10.1007/S10934-025-01854-2.

57 M. Mini, D. Jayakumar and P. Kumar, In-silico and in-vitro assessment of the antibiofilm potential of azo dye, carmoisine against Pseudomonas aeruginosa, *J. Biomol. Struct. Dyn.*, 2024, **42**, 6700–6710, DOI: 10.1080/07391102.2023.2237579.

58 K. Verma and R. Prasad, Molecular modeling of azo-food dye metabolites in the brain and their effects on attention deficit and hyperactivity disorder (ADHD) using ArgusLab software, *J. Food Saf. Hyg.*, 2024, **10**, 270–283, DOI: 10.18502/JFSH.V10I4.19392.

59 G. M. Mamardashvili, E. Y. Kaigorodova, I. S. Lebedev and N. Z. Mamardashvili, Axial complexes of Sn(IV)-tetra(4-sulfophenyl)porphyrin with azorubine in aqueous media: Fluorescent probes of local viscosity and pH indicators, *J. Mol. Liq.*, 2022, **366**, 120277, DOI: 10.1016/J.MOLLIQ.2022.120277.

60 M. Karami and M. Shabani-Nooshabadi, Electro-sensing of carmoisine and tartrazine in foodstuffs based on triple-shell CaMgFe2O4 hollow spheres-modified sensor, *Mater. Chem. Phys.*, 2024, **318**, 129289, DOI: 10.1016/J.MATCHEMPHYS.2024.129289.

61 T. N. Alenazi, H. H. Alsharief, A. Almahri, H. K. Al-Zahrani, H. A. Katuah, R. Shah, F. A. Saad and N. M. El-Metwaly, Optimization on the heterogeneous photocatalytic degradation of Azorubine E122 dye using nanocomposite *via* CuO nanoparticles with sodium mordenite, *J. Mol. Liq.*, 2024, **396**, 123926, DOI: 10.1016/J.MOLLIQ.2023.123926.

62 N. S. Abdullah, M. A. Hassan and R. O. Hassan, A Novel Flow Injection Method with Chemiluminescence Detection for the Determination of Carmoisine in Gelatin Desserts, *J. Fluoresc.*, 2024, **35**(5), 3405–3413, DOI: 10.1007/S10895-024-03777-8.

63 M. Haque, J. Chutia, A. Mondal, S. Quraishi, K. Kumari, E. W. M. Marboh, K. Aguan and A. Singha Roy, Formation of CdTe core and CdTe@ZnTe core–shell quantum dots *via* hydrothermal approach using dual capping agents: deciphering the food dye sensing and protein binding applications, *Phys. Chem. Chem. Phys.*, 2024, **26**, 22941–22958, DOI: 10.1039/D4CP02225D.

64 G. M. Nabil, M. E. Mahmoud and S. O. Makled, Green synthesis of novel magnetite mixed metal oxides with cationic surfactant nanocomposite: Investigation of its effective removal of Azorubine E122 food dye and

antimicrobial activity, *Appl. Organomet. Chem.*, 2023, **37**, e6996, DOI: 10.1002/AOC.6996.

65 I. Ali, T. Kon'kova, E. Liberman, E. Simakina, Z. A. ALOthman, T. S. Alomar and M. Ataul Islam, Preparation and characterization of SnO2-CeO2 nanocomposites: Sorption, modeling and kinetics for azorubine dye removal in water, *J. Mol. Liq.*, 2022, **346**, 117119, DOI: 10.1016/J.MOLLIQ.2021.117119.

66 K. Labiod, S. Hazourli, M. Bendaia, M. Tlili, A. Aitbara, R. Graine and H. Meradi, Removal of Azo Dye Carmoisine by Adsorption Process on Diatomite, *Adsorpt. Sci. Technol.*, 2022, 9517605, DOI: 10.1155/2022/9517605.

67 M. A. Akl, A. G. Mostafa, M. Y. Abdelaal and M. A. K. Nour, Surfactant supported chitosan for efficient removal of Cr(VI) and anionic food stuff dyes from aquatic solutions, *Sci. Rep.*, 2023, **13**(1), 1–27, DOI: 10.1038/s41598-023-43034-9.

68 P. Mohammadzadeh Jahani, F. G. Nejad, R. Zaimbashi, S. Tajik, S. Z. Mohammadi and H. Beitollahi, Electrochemical sensor based on Zn-Co zeolitic imidazolate framework/graphitic carbon nitride nanocomposite for sensitive detection of carmoisine, *Int. J. Environ. Anal. Chem.*, 2025, 2569815, DOI: 10.1080/03067319.2025.2569815.

69 B. Kharisov, O. Kharissova, V. Zhinzhilo, J. Bryantseva and I. Uflyand, Solid-Phase Extraction of Organic Dyes on Mixed-Ligand Zr(IV) Metal–Organic Framework, *Appl. Sci.*, 2022, **12**, 12219, DOI: 10.3390/APP122312219.

70 C. Burukai, B. Nyoni, D. Nyama, C. Mpofu, B. Hlabano-Mayo, B. Yalala, J. I. Mnyango and S. P. Hlan, Effectiveness of African Wattle Tree (Peltophorum africanum) Biochar in Removing Carmoisine Dye from Wastewater, *Asian J. Chem.*, 2025, pp. 2281–2290. https://www.researchgate.net/profile/Jabulani-Mnyango/publication/395099267_Effectiveness_of_African_Wattle_Tree_Peltophorum_africanum_Biochar_in_Removing_Carmoisine_Dye_from_Wastewater/links/68b325a6d9261f6f51b05236/Effectiveness-of-African-Wattle-Tree-Peltophorum-africanum-Biochar-in-Removing-Carmoisine-Dye-from-Wastewater.pdf, accessed November 9, 2025.

71 H. J. Abboud, Z. H. Mahmoud, A. M. Saadoun, E. A. A. Kareem, M. Mudhafar, Q. R. Lahhob and R. M. Mhaib, MoS_2 nanosheets-modified screen-printed electrode for the simultaneous detection of carmoisine and tartrazine, *J. Electrochem. Sci. Eng.*, 2025, **15**, 2620, DOI: 10.5599/jese.2620.

72 S. Sunil and B. K. Mandal, Facile synthesis of CQD/g-C3N4 as a highly effective metal-free photocatalyst for the degradation of carmoisine and indigo carmine dye, *Inorg. Chem. Commun.*, 2025, **171**, 113545, DOI: 10.1016/J.INOCHE.2024.113545.

73 A. K. Karan, D. Sahoo, S. Sen, S. Rakshit and N. B. Manik, Modification of barrier height inhomogeneity in the presence of titanium dioxide nanoparticles on Carmoisine dye-based Schottky device, *Surf. Interfaces*, 2024, **46**, 103952, DOI: 10.1016/J.SURFIN.2024.103952.

74 E. M. Doroh, R. S. Khoshnood, D. S. Khoshnoud and Z. Es'haghi, Photocatalytic degradation of azorubine dye in aqueous solutions using Bismuth Ferrite nanopowders, *Surf. Interfaces*, 2023, **18**, 107–122, DOI: 10.22075/CHEM.2022.27758.2085.

75 M. M. Sajid, T. Alomayri and H. Zhai, Facile synthesis of novel CoWO4/FeWO4 hetrocomposite with efficient visible light photocatalytic degradation and hydrogen evolution aspects, *J. Taibah Univ. Sci.*, 2023, **17**, 2265631, DOI: 10.1080/16583655.2023.2265631.

76 S. Landi, I. R. Segundo, C. Afonso, O. Lima, M. F. M. Costa, E. Freitas and J. Carneiro, Evaluation of band gap energy of TiO2 precipitated from titanium sulphate, *Phys. B Condens. Matter*, 2022, **639**, 414008, DOI: 10.1016/J.PHYSB.2022.414008.

77 A. D. Kusumah, Y. Yulizar, D. O. B. Apriandanu and R. M. Surya, Fabrication of ZnO and ZnO/CuMoO4 for the improvement of photocatalytic performance, *Vacuum*, 2024, **222**, 113034, DOI: 10.1016/J.VACUUM.2024.113034.

78 J. Sharmila, S. Suresh and M. Chamundeeswari, Acute toxicology study of organic dyes-degraded water on adult zebrafish as human model for direct utility, *Environ. Dev. Sustain.*, 2024, **27**(8), 18655–18674, DOI: 10.1007/S10668-024-04710-6.

79 A. Wakrim, Z. Zaroual, S. El Ghachtouli, J. J. Eddine and M. Azzi, Treatment and Degradation of Azo Dye Waste Industry by Electro-Fenton Process, *Phys. Chem. Res.*, 2022, **10**, 495–504, DOI: 10.22036/PCR.2022.315931.1991.

80 L. L. G. Al-mahamad and M. M. A. Almijbilee, Spectrophotometric analysis of the degradation products of carmoisine azo dye after removing from aqueous solutions, *J. Indian Chem. Soc.*, 2025, **102**, 101950, DOI: 10.1016/J.JICS.2025.101950.

81 E. Guerra, F. Gosetti, E. Marengo, M. Llompart and C. Garcia-Jares, Study of photostability of three synthetic dyes commonly used in mouthwashes, *Microchem. J.*, 2019, **146**, 776–781, DOI: 10.1016/J.MICROC.2019.02.002.

82 V. B. Shevale, A. G. Dhodamani, V. B. Koli, R. P. Barkul, J. P. Jadhav and S. D. Delekar, Efficient degradation of Azorubin S colourant in the commercial jam-jelly food samples using TiO2-CoFe2O4 nanocomposites in visible light, *Mater. Res. Bull.*, 2017, **89**, 79–88, DOI: 10.1016/J.MATERRESBULL.2017.01.012.

83 A. Mohagheghian, K. Ayagh, K. Godini and M. Shirzad-Siboni, Improved photocatalytic removal of Acid Red 14 by amino-functionalized Fe3O4–WO3 nanoparticles from aqueous solutions in the presence of UV irradiation, *Desalination Water Treat.*, 2017, **74**, 371–382, DOI: 10.5004/DWT.2017.20593.

84 S. B. Nehru, N. Perumal and Y. P. Subbarayalu, Sustainable water treatment: Synthesis and characterization of g-C3N5/NiCo2S4 heterojunction nanocomposite for efficient visible light-induced degradation of highly hazardous organic pollutants, *J. Water Proc. Eng.*, 2025, **73**, 107712, DOI: 10.1016/J.JWPE.2025.107712.

85 H. Salari and M. Kohantorabi, Heterogeneous photocatalytic degradation of organic pollutant in

aqueous solutions by S-scheme heterojunction in nickel molybdate nanocomposites, *J. Environ. Chem. Eng.*, 2021, **9**, 105903, DOI: 10.1016/J.JECE.2021.105903.

86 M. Shams, H. Balouchi, H. Alidadi, F. Asadi, E. K. Goharshadi, S. Rezania, S. Rtimi, I. Anastopoulos, Z. Bonyadi, K. Mehranzamir and D. A. Giannakoudakis, Coupling electrocoagulation and solar photocatalysis for electro- and photo-catalytic removal of carmoisine by Ag/graphitic carbon nitride: Optimization by process modeling and kinetic studies, *J. Mol. Liq.*, 2021, **340**, 116917, DOI: 10.1016/J.MOLLIQ.2021.116917.

87 A. E. Alprol, A. Bakr, S. I. Al-Saeedi, E. El-Haroun and M. Ashour, Sunlight-driven degradation of acid red 14 using a ZnO-doped carbon-ammonia composite: kinetics, equilibrium, and thermodynamic studies, *Front. Mar. Sci.*, 2025, **12**, 1624235, DOI: 10.3389/FMARS.2025.1624235/FULL.

88 I. Ali, T. Kon'kova, E. Liberman, A. Gaydukova, T. Agustiono Kurniawan, S. A. Aldossari, G. Imanova and X. Y. Mbianda, Recycling and characterization of spent catalyst: Carmoisine dye removal from water and carbon monoxide conversion to carbon dioxide in air, *Inorg. Chem. Commun.*, 2024, **167**, 112747, DOI: 10.1016/J.INOCHE.2024.112747.

89 I. V. Zagaynov, E. Y. Liberman, A. V. Naumkin, Y. Wai, A. A. Konovalov, E. A. Obraztsova and D. A. Kirilenko, Catalytic performance of Cu-Mn-Ce-O solid solutions doped with iron triad metals, *Mol. Catal.*, 2025, **584**, 115272, DOI: 10.1016/J.MCAT.2025.115272.

90 R. Shaheen and M. A. Hanif, High speed removal of toxic acid red dye using photocatalytic-hybrid composite material, *Desalination Water Treat.*, 2024, **317**, 100153, DOI: 10.1016/J.DWT.2024.100153.

91 M. Arif, Photocatalytic degradation of dyes by metal sulfide–chitosan based composites: a comprehensive review, *RSC Adv.*, 2026, **16**, 5353–5373, DOI: 10.1039/d5ra07777j.

92 Z. Kiayi, T. B. Lotfabad, A. Heidarinasab and F. Shahcheraghi, Microbial degradation of azo dye carmoisine in aqueous medium using Saccharomyces cerevisiae ATCC 9763, *J. Hazard. Mater.*, 2019, **373**, 608–619, DOI: 10.1016/J.JHAZMAT.2019.03.111.

93 S. Khataee, G. Dehghan, R. Yekta, S. Rashtbari, S. Maleki and A. Khataee, The protective effect of natural phenolic compound on the functional and structural responses of inhibited catalase by a common azo food dye, *Food Chem. Toxicol.*, 2022, **160**, 112801, DOI: 10.1016/J.FCT.2021.112801.

94 P. Hassanvand, M. Rajabi, T. B. Lotfabad and S. Yaghmaei, Interaction between the electrochemical properties of powdered activated carbon and the biochemical processes within bacteria in Azo dye biodecolorization: An explanatory mechanism, *Process Biochem.*, 2024, **146**, 498–508, DOI: 10.1016/J.PROCBIO.2024.09.025.

95 J. Trawiński and R. Skibiński, Stability of aspartame in the soft drinks: Identification of the novel phototransformation products and their toxicity evaluation, *Food Res. Int.*, 2023, **173**, 113365, DOI: 10.1016/J.FOODRES.2023.113365.

96 M. Ahmadi and F. Ghanbari, Degradation of organic pollutants by photoelectro-peroxone/ZVI process: Synergistic, kinetic and feasibility studies, *J. Environ. Manage.*, 2018, **228**, 32–39, DOI: 10.1016/J.JENVMAN.2018.08.102.

97 M. R. Sohrabi, A. Khavaran, S. Shariati and S. Shariati, Removal of Carmoisine edible dye by Fenton and photo Fenton processes using Taguchi orthogonal array design, *Arab. J. Chem.*, 2017, **10**, S3523–S3531, DOI: 10.1016/J.ARABJC.2014.02.019.

98 K. Biswas, Z. Ahamed, T. Dutta, B. Mallick, A. R. Khuda-Bukhsh, J. K. Biswas and S. K. Mandal, Green synthesis of silver nanoparticles from waste leaves of tea (Camellia sinensis) and their catalytic potential for degradation of azo dyes, *J. Mol. Struct.*, 2024, **1318**, 139448, DOI: 10.1016/J.MOLSTRUC.2024.139448.

99 M. R. Eskandarian, M. Ganjkhanloo, M. H. Rasoulifard and S. A. Hosseini, Energy-efficient removal of acid red 14 by UV-LED/persulfate advanced oxidation process: Pulsed irradiation, duty cycle, reaction kinetics, and energy consumption, *J. Taiwan Inst. Chem. Eng.*, 2021, **127**, 129–139, DOI: 10.1016/J.JTICE.2021.07.035.

100 A. Wakrim, A. Dassaa, Z. Zaroual, S. El Ghachtouli, J. Jamal Eddine and M. Azzi, Mechanistic study of carmoisine dye degradation in aqueous solution by Fenton process, *Mater. Today Proc.*, 2021, **37**, 3847–3853, DOI: 10.1016/J.MATPR.2020.08.405.

101 L. Micheletti, B. Coldibeli, C. A. R. Salamanca-Neto, L. C. Almeida and E. R. Sartori, Assessment of the use of boron-doped diamond electrode for highly sensitive voltammetric determination of the azo-dye carmoisine E-122 in food and environmental matrices, *Talanta*, 2020, **220**, 121417, DOI: 10.1016/J.TALANTA.2020.121417.

102 J. M. Obón, J. M. Angosto, F. González-Soto, A. Ascua and J. A. Fernández-López, Prototyping a spinning adsorber submerged filter for continuous removal of wastewater contaminants, *J. Water Proc. Eng.*, 2022, **45**, 102515, DOI: 10.1016/J.JWPE.2021.102515.

103 M. Zulfajri, M. Adlim, N. Andalia, A. Rasool, S. Sudewi and G. G. Huang, Preparation of magnesium acetate-modified pineapple crown waste hydrochar *via* co-hydrothermal carbonization for a specific azo dye adsorption, *Bioresour. Technol. Rep.*, 2025, **30**, 102127, DOI: 10.1016/J.BITEB.2025.102127.

104 S. Madihi-Bidgoli, S. Asadnezhad, A. Yaghoot-Nezhad and A. Hassani, Azurobine degradation using Fe2O3@multi-walled carbon nanotube activated peroxymonosulfate (PMS) under UVA-LED irradiation: performance, mechanism and environmental application, *J. Environ. Chem. Eng.*, 2021, **9**, 106660, DOI: 10.1016/J.JECE.2021.106660.

105 F. Garkani Nejad, I. Sheikhshoaie and H. Beitollahi, Simultaneous detection of carmoisine and tartrazine in food samples using GO-Fe3O4-PAMAM and ionic liquid

based electrochemical sensor, *Food Chem. Toxicol.*, 2022, **162**, 112864, DOI: 10.1016/J.FCT.2022.112864.

106 D. D. Tuan, W. Da Oh, F. Ghanbari, G. Lisak, S. Tong and K. Y. Andrew Lin, Coordination polymer-derived cobalt-embedded and N/S-doped carbon nanosheet with a hexagonal core-shell nanostructure as an efficient catalyst for activation of oxone in water, *J. Colloid Interface Sci.*, 2020, **579**, 109–118, DOI: 10.1016/J.JCIS.2020.05.033.

107 F. Abbaci, A. Nait-Merzoug, O. Guellati, A. Harat, J. El Haskouri, J. Delhalle, Z. Mekhalif and M. Guerioune, Bio/KOH ratio effect on activated biochar and their dye based wastewater depollution, *J. Anal. Appl. Pyrolysis*, 2022, **162**, 105452, DOI: 10.1016/J.JAAP.2022.105452.

108 M. Hasanpour, M. Shirzad-Siboni, K. Ayagh and A. Mohagheghian, Adsorption of acid red 14 from aqueous solutions by ZnO-tyre: kinetics, isotherms, and mechanisms, *Int. J. Environ. Anal. Chem.*, 2024, **105**, 5083–5109, DOI: 10.1080/03067319.2024.2384648.

109 S. Shen, H. Li, J. jia Fu and H. B. Wang, Wastewater purification with different precursors of carbon dots dominated titanium dioxide: Mechanism insight, *J. Alloys Compd.*, 2022, **922**, 166162, DOI: 10.1016/J.JALLCOM.2022.166162.

110 R. M. A. Q. Jamhour, A. M. Al-Msiedeen, R. Z. Al-Sharaydeh, M. R. Jamhour and A. M. Altweiq, Zn-Al layered double hydroxide nanoparticles for efficient removal of food dyes from wastewater, *Desalination Water Treat.*, 2024, **317**, 100036, DOI: 10.1016/J.DWT.2024.100036.

111 A. Sadeghi, M. H. Ehrampoush, M. T. Ghaneian, A. A. Najafpoor, H. Fallahzadeh and Z. Bonyadi, The effect of diazinon on the removal of carmoisine by Saccharomyces cerevisiae, *Desalination Water Treat.*, 2019, **137**, 273–278, DOI: 10.5004/DWT.2019.23189.

112 M. S. Kafshgari, M. Jahanshahi and M. Ghorbani, Magnetic coordination polymer for dye removal and antibacterial activity, *J. Taiwan Inst. Chem. Eng.*, 2023, **149**, 104995, DOI: 10.1016/J.JTICE.2023.104995.

113 M. Shams, S. Abd Mojiri, M. Shafaee, N. E. Hassan, A. Dehghan, M. Baziar, E. K. Goharshadi and S. Rezania, BiOI-MIL Binary Composite for Synergistic Azo Dye AR14 Discoloration, *Catalysts*, 2025, **15**, 26, DOI: 10.3390/CATAL15010026/S1.

114 D. Pan, N. Parshi, B. Jana, K. Prasad and J. Ganguly, Optimization of the spontaneous adsorption of food colors from aqueous medium using functionalized Chitosan/Cinnamaldehyde hydrogel, *Int. J. Biol. Macromol.*, 2021, **193**, 758–767, DOI: 10.1016/J.IJBIOMAC.2021.10.187.

115 D. Saloglu and O. I. Sahin, Removal of azo dyes – tartrazine, carmoisine, and Allura Red – from wastewater using Spirulina biomass-immobilized alginate beads: equilibrium, kinetics, thermodynamics, desorption, and reusability, *Desalination Water Treat.*, 2021, **220**, 431–445, DOI: 10.5004/DWT.2021.27010.

116 Z. Ulker, R. Bozbay, S. D. Buyuk and N. Orakdogen, Eco-friendly property modulation of biobased gels of carboxymethyl cellulose-integrated poly(tertiary amine)s for the removal of azo-food dyes, *Int. J. Biol. Macromol.*, 2024, **282**, 137199, DOI: 10.1016/J.IJBIOMAC.2024.137199.

117 K. Devi, D. Rawat, L. Chopra, Manikanika, K. Pal, M. E. A. Mohsin and S. Mousa, Fe3O4@starch nanocomposites: A photocatalyst for efficient degradation of rhodamine B and acid red 114, *Int. J. Biol. Macromol.*, 2025, **318**, 144564, DOI: 10.1016/J.IJBIOMAC.2025.144564.

118 F. Shahverdi and M. R. Shahverdi, Optimizing the Removal of Acid Red 14 Onto Chitosan-Based Electrospun Nanofibers Using Surface Response Technique: Adsorption Kinetic Studies Using Linear and Nonlinear Approaches, *Fibers Polym.*, 2025, **26**(9), 3951–3962, DOI: 10.1007/S12221-025-01050-8.

119 R. M. Abdelaziz, A. El-Maghraby, W. A. A. Sadik, A. G. M. El-Demerdash and E. A. Fadl, Biodegradable cellulose nanocrystals hydrogels for removal of acid red 8 dye from aqueous solutions, *Sci. Rep.*, 2022, **12**(1), 1–17, DOI: 10.1038/s41598-022-10087-1.

120 V. K. Gupta, A. Mittal, A. Malviya and J. Mittal, Adsorption of carmoisine A from wastewater using waste materials—Bottom ash and deoiled soya, *J. Colloid Interface Sci.*, 2009, **335**, 24–33, DOI: 10.1016/J.JCIS.2009.03.056.

121 S. Mousavi, F. Shahraki, M. Aliabadi, A. Haji, F. Deuber and C. Adlhart, Nanofiber immobilized CeO2/dendrimer nanoparticles: An efficient photocatalyst in the visible and the UV, *Appl. Surf. Sci.*, 2019, **479**, 608–618, DOI: 10.1016/J.APSUSC.2019.02.119.

122 M. I. Khan, S. A. Yahya, A. ElKhaleefa, I. Shigidi, I. H. Ali, M. Rehan and A. M. Pirzada, Toxic Anionic Azo Dye Removal from Artificial Wastewater by Using Polyaniline/Clay Nanocomposite Adsorbent: Isotherm, Kinetics and Thermodynamic Study, *Processes*, 2025, **13**, 13, DOI: 10.3390/pr13030827.

123 S. Jana, J. Ray, B. Mondal, S. S. Pradhan and T. Tripathy, pH responsive adsorption/desorption studies of organic dyes from their aqueous solutions by katira gum-cl-poly(acrylic acid-co-N-vinyl imidazole) hydrogel, *Colloids Surf., A*, 2018, **553**, 472–486, DOI: 10.1016/J.COLSURFA.2018.06.001.

124 W. J. Li, X. Zhou, S. S. Tong and Q. Jia, Poly(*N*-isopropylacrylamide-co-N,N′-methylene bisacrylamide) monolithic column embedded with γ-alumina nanoparticles microextraction coupled with high-performance liquid chromatography for the determination of synthetic food dyes in soft drink samples, *Talanta*, 2013, **105**, 386–392, DOI: 10.1016/J.TALANTA.2012.10.065.

125 I. V. Zagaynov, I. V. Shelepin, E. Y. Liberman, N. R. Arutyunyan and A. A. Konovalov, Ceria doped with trivalent cations in advanced oxidation process, *Mater. Lett.*, 2025, **396**, 138801, DOI: 10.1016/J.MATLET.2025.138801.

126 S. K. Tammina, B. K. Mandal and F. N. Khan, Mineralization of toxic industrial dyes by gallic acid mediated synthesized photocatalyst SnO2 nanoparticles,

Environ. Technol. Innov., 2019, **13**, 197–210, DOI: 10.1016/J.ETI.2018.11.004.

127 R. Martínez-Moro, M. del Pozo, E. Casero, M. D. Petit-Domínguez and C. Quintana, MoS2 quantum dots-based optical sensing platform for the analysis of synthetic colorants. Application to quinoline yellow determination, *Spectrochim. Acta, Part A*, 2023, **302**, 123042, DOI: 10.1016/J.SAA.2023.123042.

128 S. I. S. Al-Hawary, R. Rahimpoor, A. Rahmani, R. M. Romero-Parra, A. A. Ramírez-Coronel, F. R. Alhachami, N. Mengelizadeh and D. Balarak, Enhanced Sonophotocatalytic Degradation of Acid Red 14 Using Fe3O4@SiO2/PAEDTC@MIL-101 (Fe) Based on Metal-Organic Framework, *Catalysts*, 2023, **13**, 411, DOI: 10.3390/CATAL13020411.

129 D. Bhatt, K. Vyas, S. Singh, P. J. John and I. P. Soni, Sunset Yellow induced biochemical and histopathological alterations in rat brain sub-regions, *Acta Histochem.*, 2024, **126**, 152155, DOI: 10.1016/J.ACTHIS.2024.152155.

130 S. Yılmazer Keskin, N. Demir, C. S. Keskin and A. Avcı, Bioacumulation and biosorption properties of Penicillium funiculosum against textile dyes, *Appl. Water Sci.*, 2025, **15**(11), 1–13, DOI: 10.1007/S13201-025-02629-5.

131 S. V. Smirnova, K. A. Lyskovtseva and I. V. Pletnev, Extraction and determination of synthetic food dyes using tetraalkylammonium based liquid-liquid extraction, *Microchem. J.*, 2021, **162**, 105833, DOI: 10.1016/J.MICROC.2020.105833.

132 L. Mattoli, G. Fodaroni, G. Proietti, E. Flamini, B. Paoli, L. Massa, G. C. Ferrara, E. Giovagnoni and M. Gianni, Biodegradability of dietary supplements: Advanced analytical methods to study the environmental fate of artificial sweeteners and dyes, *J. Pharm. Biomed. Anal.*, 2025, **255**, 116575, DOI: 10.1016/J.JPBA.2024.116575.

133 Y. Sukhatskiy, R. Mnykh, V. Tsymbaliuk, M. Shepida, M. Sozanskyi and Z. Znak, Ultrasound-assisted synthesis of Cu2O nanoparticles-clinoptilolite composites: Characterization, antifungal activity, and effectiveness in sonocatalytic periodate activation for oxidative degradation of acid red 14 dye, *J. Water Proc. Eng.*, 2025, **74**, 107792, DOI: 10.1016/J.JWPE.2025.107792.

134 N. M. Mahmoodi and M. Arami, Bulk phase degradation of Acid Red 14 by nanophotocatalysis using immobilized titanium(IV) oxide nanoparticles, *J. Photochem. Photobiol., A*, 2006, **182**, 60–66, DOI: 10.1016/J.JPHOTOCHEM.2006.01.014.

135 M. Abdullah, H. Bakhtiar, G. Krishnan, M. S. A. Aziz, W. H. Danial and S. Islam, Transition from saturable absorption to reverse saturable absorption of carmoisine dye under low-powered continuous wave laser excitation, *Opt. Laser Technol.*, 2019, **115**, 97–103, DOI: 10.1016/J.OPTLASTEC.2019.01.032.

136 N. Kaneva, S. Petrova and A. Bachvarova-Nedelcheva, Photocatalytic Decomposition of Carmoisine and Crystal Violet by Ho-Doped TiO2 Sol-Gel Powders, *Materials*, 2026, **19**(19), 17, DOI: 10.3390/ma19010017.

137 H. M. Meena, S. Kukreti and P. S. Jassal, Study on adsorptive removal of carmoisine azo dye from aqueous solution using the modification of activated carbon from rubber fruit shells and its magnetic composite, *Mater. Res. Innovations*, 2025, DOI: 10.1080/14328917.2025.2600256.